SYNTHESIS, PROPERTY STUDY AND MODIFICATION OF II-VI SULFIDE SEMICONDUCTOR NANOPARTICLES

By

TONG NI

Bachelors of Science
Lanzhou University
Lanzhou, Gansu P.R.China
1992

Masters of Science
Lanzhou University
Lanzhou, Gansu P.R.China
1995

Submitted to the Faculty of the
Graduate College of the
Oklahoma State University
in partial fulfillment of
the requirement for
the Degree of MASTERS OF SCIENCE
May, 2000

SYNTHESIS, PROPERTY STUDY AND

MODIFICATION OF II-VI SULFIDE

SEMICONDUCTOR

NANOPARTICLES

Thesis approved:

Thesis Advisor

Dean of the Graduate College

PREFACE

Surface modification of semiconductor nanoparticle material would not only improve the stability but also its performance. This study is devoted to new synthetic methods for preparation and modification of hydrophilic semiconductor CdS, CdSe nanoparticles resulting in a novel type of compounds-supramolecules, resembles of metal complexes and nanoparticles. A variety of spectroscopic methods were used to monitor the modification process and to investigate the optical properties of the supramolecules.

Based on the consideration of the structure of nanoparticles, a Lewis acid CuBM was chosen for the modification of S sites on the particle surface. XRD, TEM, UV-Vis, XPS, ^{1}H NMR, EPR, photoluminescence and time-resolved fluorescence were used to study the modification, and a structure was proposed based on the spectroscopic results. The modification was found to be light induced and reversible.

ACKNOWLEDGMENTS

I would like to express deep appreciation to my research adviser, Dr. Nicholas Kotov for his guidance, instruction, suggestions and his strong interest in the progress of my research. I wish to express my sincere gratitude t him for providing me with excellent research facilities, sharing knowledge and support. I am also grateful to Dr. Zaid El Rassi and Dr. Allen Apblett for serving on my graduate committee.

l would like to thank Dr. Margarete Eastman, Dr. Luis M. Liz Marzan, Dr. Jim Packett and Mr. Gordon H. Gainer for taking NMR, XPS, XRD and time-resolved fluorescence spectrum (TRPL) for me, and also for their helpful discussion on results interpretations. I would like to thank Mr. Dattatri K Nagesha, Mr. Arif Mamedov, Mr. John Ostrander, Mrs. Natasha Mamedova and the other in the group for their help and friendship.

Finally, I would to acknowledge the Department of Chemistry of OSU for providing me an opportunity to continue my education and the financial support.

I would like to express my special thanks to my mother Mrs. Shunqing Xue, my father Mr. Mingkang Ni, my sister Mrs. Xiaojun Ni for the love, understanding, motivation, support and encouragement.

TABLE OF CONTENTS

LIST OF SCHEMES

LIST OF TABLES

LIST OF FIGURES

Chapter I

Chapter II

Chapter III

Figure Page

NOMENCLATURE

nm	Nanometer
λ	Wavelength
TOP	Tri-n-octylphosphine
TOPO	Tri-n-octylphosphine oxide
SEC	Size exclusion chromatography
TEM	Transmission electron microscopy
XRD	X ray diffraction
NMR	Nuclear magnetic resonance
ESR	Electron spin resonance
XPS	X ray photoelectron spectroscopy
TRPL	Time resolved photoluminescence
E_g	Band gap energy
eV	Electron volts
CdS-citrate	CdS nanoparticles stabilized by sodium citrate
CuBM	(2,2'-bipyridyl-N,N')(malonato-O,O')-copper(II) monohydrate
ns	Nanosecond

CHAPTER I

INTRODUCTION

A. NANOPARTICLES AND THEIR APPLICATIONS

Nanoparticles are typically defined as inorganic or organic molecular structures with diameters ranging from 1 nm to 100 nm. They have been the subject of intense scientific and technological activity for over a decade. These species display properties intermediate between single molecules and bulk materials, and can be made from a variety of materials such as metals metal oxides, sulfides, selenides, ceramics, polymers, etc.. In the fundamental research the greatest attention was paid to the so called II-VI semiconductor nanoparticles, i.e. sulfides and selenides of two valence electron metals represented by CdS, CdSe. For them, the range of nanoparticle diameters for which the size effect on properties is the most pronounced, is set by the characteristic length of Wannier exciton-the distance of correlated motion of electron/hole pair. Depending on a particular II-VI semiconductor this size falls between the range of 1 and 10 nm, correspondingly, most of the research is being done with CdS and CdSe particles of that size.

Nanoparticles can be dispersed in water or organic solvents producing clear solution. Due to their remarkable optical, magnetic and electrical properties, high surface areas, and interface-dominate chemical properties, they are considered for a large variety of new devices, coatings, and reagents with ultra-fine sizes. Taking into account a short history of nanoparticle studies, they have been tested for wide variety of applications including

Nanoparticles can be used for targeted or controlled delivery of lipophilic or hydrophilic drug substance. Their stability and bioactivity can be increased through the surface derivatization or modification, which could also result in new therapeutic effects as well. Biodegradable nanoparticles (poly-D,L-lactic acid and poly-L-lysine-graft-polysaccharide copolymers) and other hydrophilic polymers[1] with a modified surface which could bind to tissues or cells of living systems have enhanced sustained release properties as delivery vehicles[2], protein-sized semiconductor nanoparticles such as CdS could be used as chemical sensors to bind with DNA and hence influence DNA biological functions and gene expression[3]. It can also be used as drug delivery system for intra-arterial localization of therapeutic agents for preventing restenosis due to its good suspensibility and easy penetration into an arterial wall without causing trauma[4]. Nanoprobes (generally gold)[5] are small enough to enter the cells of living system yet electron dense enough to be detected once inside and they can form tight complex with biomolecules in ways that preserve their biological functions. The ability of gold to act as photon and electron antennae make it the most sensitive reagents for detecting biological molecules for diagnostic purposes. Superparamagnetic dextran nanoparticles-DMNP[6] and γ-Fe_3O_4[7] surrounded by a primary coating of synthetic polymer and an outer polymer coating for targeting the particles to specific tissues can be used as diagnostic contrast agents and carriers for drugs, etc..

2) Chemical: Colloidal metal (embedded metals)[8], metal oxides and semiconductor solutions such as TiO_2, ZnO and ion oxides can be applied as catalysts[9, 10] for free radical reactions initiated by light or ionizing radiation; Pt, Pd, Ag and Au nanoparticles supported on α-Al_2O_3[11] are observed to have enhanced catalytic properties under lower temperature in CO oxidation and NO reduction; zinc doped Ag, Pd, Au nanoparticles are found to increase

reactivity toward CCl_4 in water, which favors fully reduced product-methane[12]; alkaline earth oxide nanoparticles (SrO, CaO)[13] and some organometallic compounds process extraordinary catalytic and reactive properties and are suggested to be used to detoxify hazardous substances such as SO_2, chlorinated hydrocarbons, insecticides, organo-phosphorous compounds or even military chemical agents.

3) Optical: Nanoparticles have vivid colors and resist deterioration better than organic pigments. They can be used as transparent conductors, filters, pigments and functional coatings and nonlinear optical switches. Light-emitting diodes represent a rapidly growing field with a significant market potential.

4) Electrical: Nanocrystalline thin films, particular hydrogenated Si films[14] are considered to be suitable candidates for thin film solar cells electronic and nanoelectronics. Other applications include capacitors, sensors, electrode materials, cosmetics for sun protection with high SPF, tracer and labeling substances, devices as information storage material due to the unique magnetic properties.

B. SYNTHESIS OF NANOPARTICLES

There have been a variety of methods to synthesize nanoparticles. The highest degree of control was achieved for wet colloidal methods of nanoparticle synthesis. Here the synthetic methods for II-VI semiconductor nanoparticles, which are the focus of this study, are surveyed. Nanoparticles can be obtained by arrested precipitation from solution before the particles grow into the bulk precipitate. The methods based on this principle include the following:

1. Reverse micelle preparation[15-20]: Surfactant such as AOT (sodium bis(ethyl-2-hexyl) sulfosuccinate), can dissolve in organic solvents and form spheroidal aggregates called reverse micelles. Water is readily solubilized in the polar core and form a water pool. The radius is dependent on $[H_2O]/[AOT]$ ratio. Sulfide nanoparticles (as well as other II-VI nanoparticles) are formed by mixing a reverse micelle containing Cd^{2+} with the other containing S^{2-} (Scheme. 1).

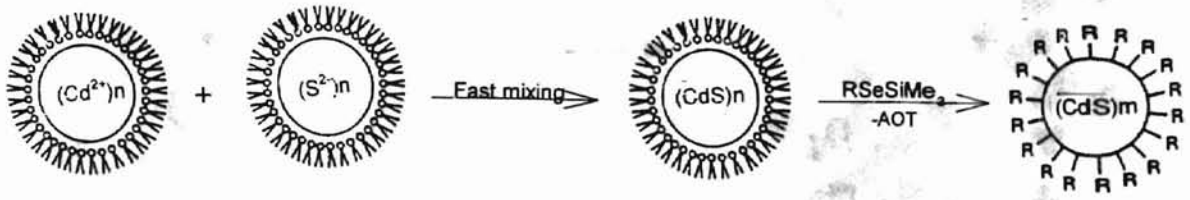

Scheme. 1 Synthesis of CdS nanoparticles in reverse micelle

The formation of nanoparticles in the water pool of reverse micelle favors the mono-dispersed particles with the size dependent on the $[H_2O]/[AOT]$ ratio. Particles in the water pool can be exchanged out of the reverse micelle by adding other hydrophobic organic compounds which could cap the nanoparticle surface and precipitate the particles out of the water pool ($RSeSiMe_3$ in scheme 1).

2. Methods based on the use of capping agents[21, 22]: Currently the most commonly used recipes of synthesis utilize the ability of some organic molecules with Lewis base character such as alcohols, glycerols, thiols, amines, phosphate, alkylphosphine oxide, citrate ion, heterocyclic compounds etc. to covalently bond to the nanoparticle surface. Such capping

controls the growth rate of particles and prevents the formation of large agglomerates (scheme 2). Despite the covalent binding, the capping agents on the nanoparticle surface can be exchanged to a new one, provided that the latter are added in a substantial excess.

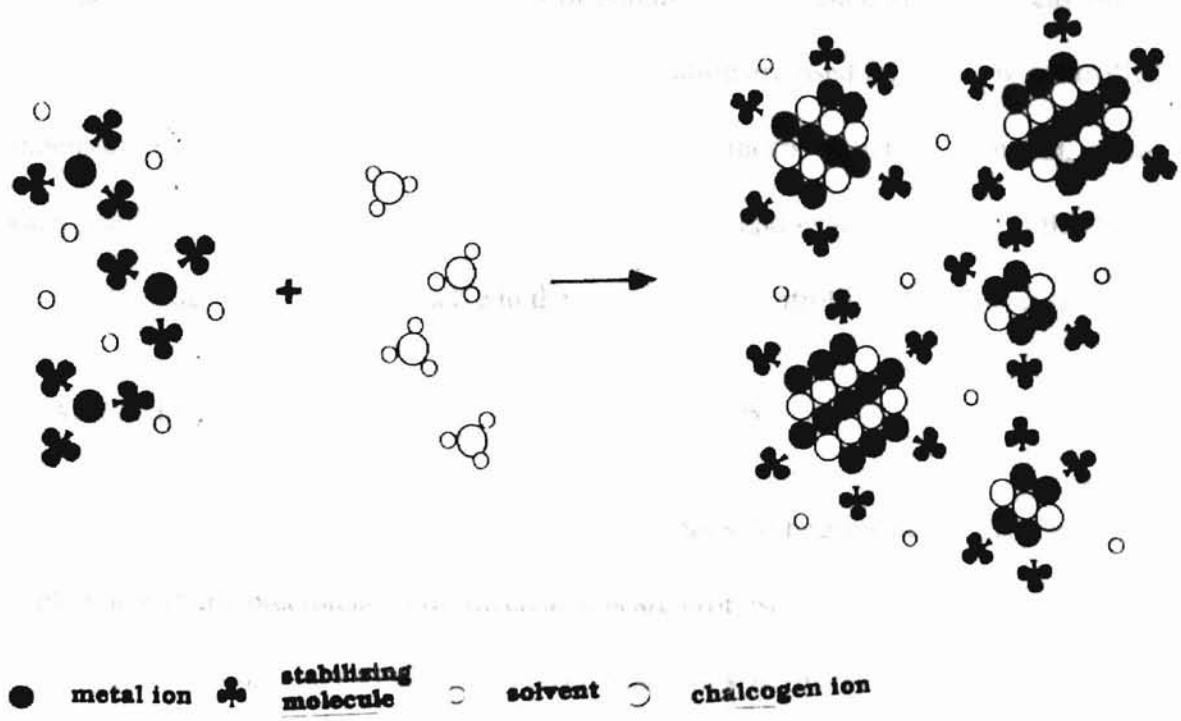

Scheme 2. Synthesis of metal sulfide nanoparticles using stabilizer

3. Sol-gel methods: Pure as well as metal-ion-doped semiconductor sulfide nanoparticles have been reported to be obtained through sol-gel methods[23,24,25], in which very small and monodispersed nanoparticles can be formed.

4.Sonication[26,27] of powdered semiconductor and magnetic materials in an organic or aqueous solvent under the atmosphere of hydrogen could also provide nanoparticle dispersions. Sulfide nanoparticles can also be prepared by sonicating metal nanoparticles with a sulfide

source in organic solvent[28]. The role of hydrogen is to prevent the formation of hydroxyl radical or any other radicals originated from sonication which is believed to be able to destroy nanoparticles through oxidation.

There are a number of "physical"methods of nanoparticle production such as gas phase synthesis in which plasma and laser induced vaporization are used followed by controlled condensation of the vapor phase. For example, the synthesis of nanoscale metal, metal oxides, carbides, and higher fullerenes, nanotubes ($MoTe_2$) and nanorods belong to this type. The disadvantage of these methods lye in the difficulty of controlling the product size.

C. PARTICLE GROWTH AND SIZE DISTRIBUTION:

Given an opportunity, metastable nanoparticles can combine to become larger until they form a bulk material and precipitate. Two mechanisms are proposed for the particle growth: the particles grow discontinuously until they reach a certain size, then Ostwald ripening takes place, i.e., larger particles grow on account of the dissolution of smaller ones. As the result, the particle size increases continuously, which is recognized as a continuous shift of the excitonic absorption band to longer wavelengths. This certain size is referred to as the "magic" agglomeration number, which is confirmed by the UV absorption maxima appearing reproducibly at the same wave length under the same synthetic conditions. Magic numbers can be either controlled thermodynamically-if certain size has particular stability-or kinetically, which is associated with the collection of nanoparticles by fast precipitation and preservation of the originally most abundant agglomeration number.

Though magic number exists, the size distribution is commonly quite wide in the colloidal

solution. As size changes, the electronic, optical, magnetic, photocatalytic properties of nanoparticles change drastically, and therefore it's important to narrow down the size distribution.

Size control and separations:

1). Some methods of synthesis are proved to be able to obtain monodispersed nanoparticles. The most widely used one is the so called TOP/TOPO[29] method. $CdMe_2$ solution in TOP (tri-n-octylphosphine) is mixed quickly with TOPSe solution in TOP at 300°C in liquid TOPO (tri-n-octylphosphine oxide) under 1 atm of argon. After the sudden temperature drop due to the introduction of TOP solutions into TOPO, the temperature was gradually elevated to 230~260°C. Different sizes hydrophobic CdSe nanoparticles with a very narrow size distribution could be obtained by changing the finial temperature.

2). Nanoparticles with wide size distribution can be redispersed in solution and separated as different size range by size selective precipitation. A solution in which nanoparticles can not be dispersed is added into the concentrated crude nanoparticles solution until the larger particles start to precipitate. The procedure is repeated several times to separate the larger particles from the smaller ones till the satisfactory mono distribution is reached. Certain amount of nanoparticles could be lost during this procedure due to formation of emulsion and simultaneous agglomeration.

3). Size selective photocorrosion[30]: is one of the methods to narrow down the size distribution. Irradiation of metal sulfide nanoparticle solution with monochromatic light at sequentially decreasing wavelengths in the presence of an electron acceptor can successfully

narrow down the size distribution and obtain decreasingly small size nanoparticles. This can be achieved only when all the photocorrosion products are soluble in aqueous solution in which the sulfide nanoparticles are present.

4). Separation of nanoparticles by size exclusion chromatography[31] (SEC) and gel electrophoresis[32]. These methods are ideal tools to study the size distribution on nanoparticles, especially SEC with a diameter ranging between 2 nm and 20 nm, and it also could be used as a potential tool for the separation of different shape (spherical and rode shape) or size nanoparticles if several problems could be successfully solved. Solid nanoparticles carrying surface charges might be considered as a special case of a polyelectrolyte, and their SEC behavior resemble charged polymers such as proteins. Better separation effects are obtained at low nanoparticle concentrations. However, a great extent irreversible adsorption of the particles onto the surface of the stationary phase is generally noticed, which is considered to result from the high surface area of stationary phase and high surface activity of nanoparticles, confirmed by the decrease in the peak area of the colloidal chromatogram peak and increasing peak width at higher concentration together with memory effect. Addition of surfactant at low concentration in the mobile phase seems to reduce this problem, while addition of an electrolyte especially polyelectrolyte seems to worsen the adsorption, well known as the depletion of the surface charges of nanoparticles and the consequent coagulation and adsorption at lowered repelling force. All effects could be explained in terms of the changing of the electrical double layer of the particles, which is responsible for the stability of the latter. Column saturated with nanoparticles (referred to as conditioned column) has been suggested for the separation study. The double layer is quite rigid and can't easily be penetrated. Therefore, thickness of the double layer which depends

on electrolyte concentration has to be taken into account when the effective diameter of a colloidal particle is considered in SEC[33, 34,35].

D. CHARACTERIZATIONS OF NANOPARTICLES

For chemical and physical properties of nanoparticles, the surface as well as their internal electron structure play an important role. The surface properties can be determined by TEM (transmission electron microscopy), small angle X-ray diffraction, nuclear magnetic resonance, atomic force microscopy, etc.. X-ray photoelectron spectroscopy (XPS), extended X-ray absorption fine structure (EXAFS) could be used to distinguish the elements from different coordination environment consisting the nanoparticles, while the optical and electronic properties can be determined by Fourier transform IR, Raman scattering[36], optical absorption (UV-vis), photo-luminescence, life-time emission measurements, etc..

1. TEM. A critical point in the evaluation of size dependent structural changes of nanoparticles is the determination of the particle's diameter. Several methods exist for this purpose but are sensitive to different size dimensions and each has some limitations. The most direct way to measure the size of nanoparticles is TEM or HREM (high resolution TEM). The size of particles can be the measured directly from the picture (Fig.1) or by counting the lattice planes when some degree of aggregation occurs. Among the limitations of TEM, one needs to mention that it is only sensitive to particles with the diameter larger than 20 Å which may lead to misinterpretations of particle size distribution.

For those extremely small clusters which are hard to be detected by TEM due to the diminishing contrast, there exists an alternative advantageous measurement - small angle X-

ray diffraction on the powdered samples. As showed in the spectrum of XRD for thioglycerol stabilized CdS nanoparticles (Fig.2), the peak angle 2θ maxima at low values ($2 \leq 2\theta \leq 10$) can be converted to the nearest neighbor distances of the clusters in the powdered samples by Bragg equation, which is considered as the diameter of the spherical particles. The broadening of peaks is noticed due to the finite crystal size strain in small particles and will affect the estimation of the particle size. The lattice pattern of nanoparticles could be obtained from the wide angle XRD. There are other methods exist to determine the particle size, with each sensitive to different size range.

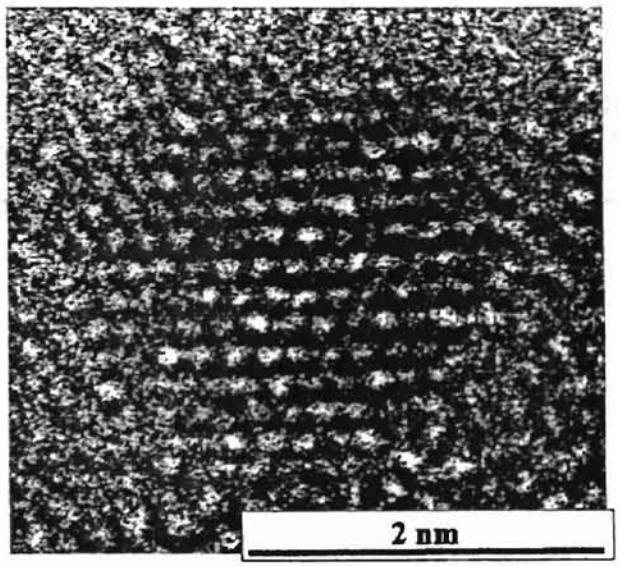

Fig.1. HREM image of ethex/DMSO stabilized CdS nanocrystal. One nearly spherical particle with a well-defined edge in the matrix with an approximate diameter of 2 nm. Black dots represent CdS atoms in the lattice

2. Quantum size effect. The key feature of II-VI semiconductor nanoparticle is the appearance of the so called quantum size effect. It's known that the band structure in metals and as well as in semiconductors is not an atomic or molecular property, but is brought about

through the periodic arrangement of a large number of atoms in a crystal lattice[37]. There exists a gradual transition from semiconductor or metal properties as the size of a crystal is successively decreased in the nanometer range.

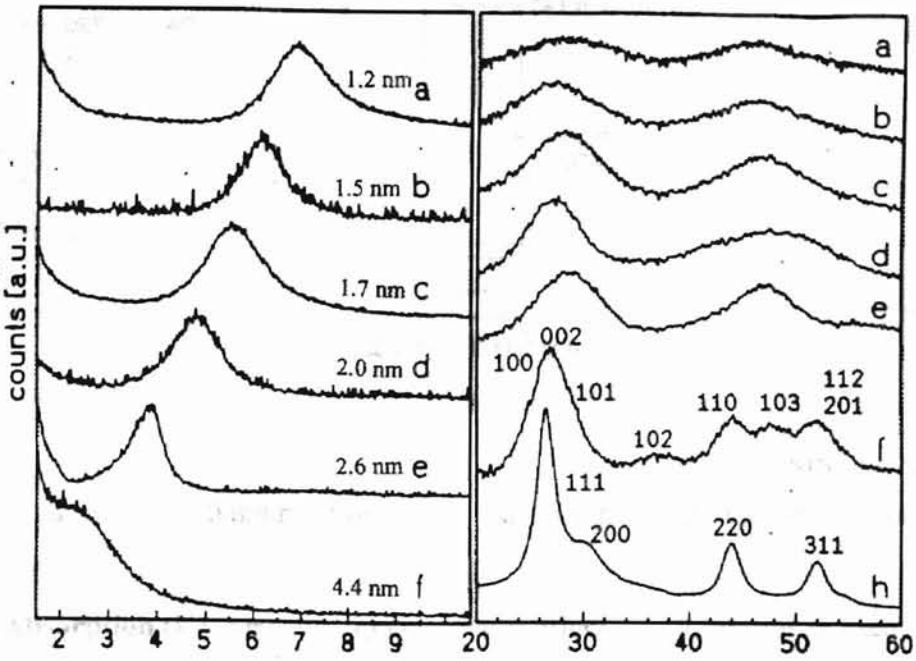

Fig. 2 Small-angle XRD (a) and wide-angle XRD (b) of powdered thioglycerol stabilized CdS nanoparticles, particle diameter increase from 1.5 nm to 10 nm through samples a to h

As shown in Fig.3, the energy spacing between the valence band and conduction band is enlarged as the particle size decreases from bulk material to nanoparticles. This gap is inversely proportional to the square of the particle diameter.

The molecules at the surface edge cause surface imperfections, which are understood as traps for electrons and holes. As the size decreases, the transition energy shifts to higher value (referred to as quantum size effect) while the surface states remain more or less the same.

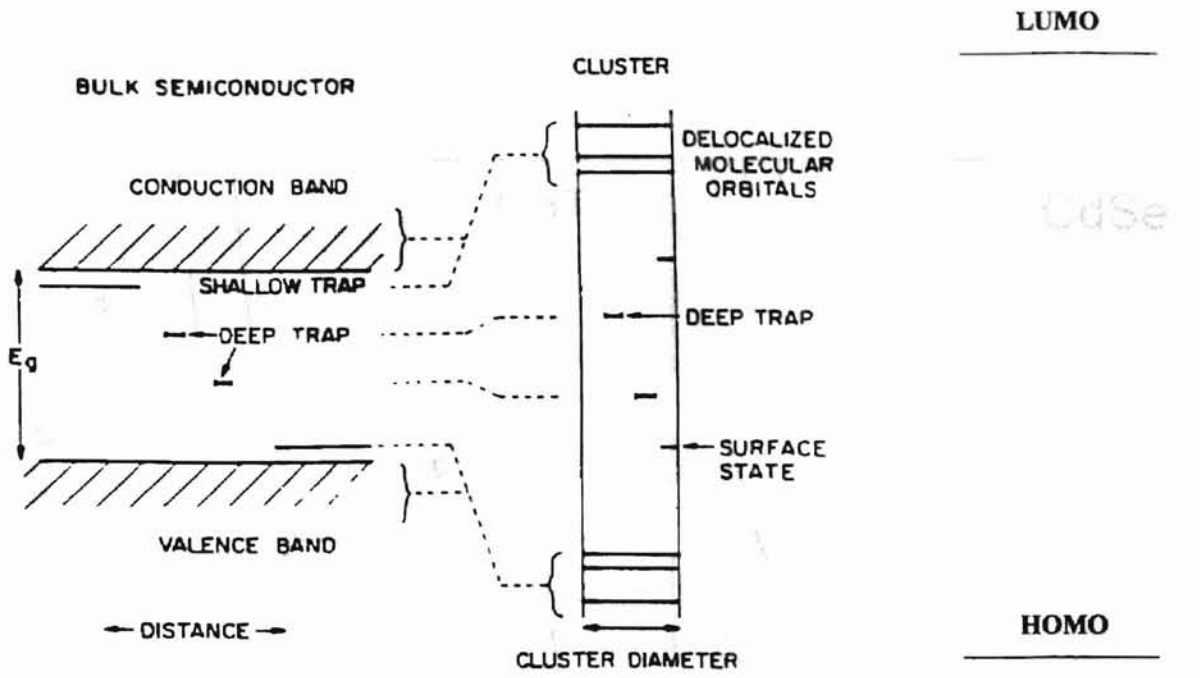

Fig.3 Electronic state diagram of bulk material, nanoparticles and single molecule

3. Optical Absorption (UV-vis). The quantum size effect has numerous consequences for the optical and catalytic properties of nanoparticles. Take the optical absorption of CdSe and CdTe nanoparticle stabilized by TOPO as an example (Fig. 4)[38].

The spectrum is featured by: 1) The absorption threshold, corresponds to the band gap energy of semiconductor nanoparticles ascribed to the first excitonic (1s-1s) transition. 2). Optical absorption reflects the quantum size effect by a blue shift as the particle size decreases. In some cases several shoulders right below the onset of the absorption can be observed and are recognized as 2nd or even higher excitonic transition. 3). Extinction coefficient. As the particles size decreases, the extinction coefficient increases. 4). Temperature dependence. With decreasing temperature, the 1s-1s transition energy shifts slightly toward higher energies. This effect is understood as the shrinking of sub energy levels in both CB and VB

bands.

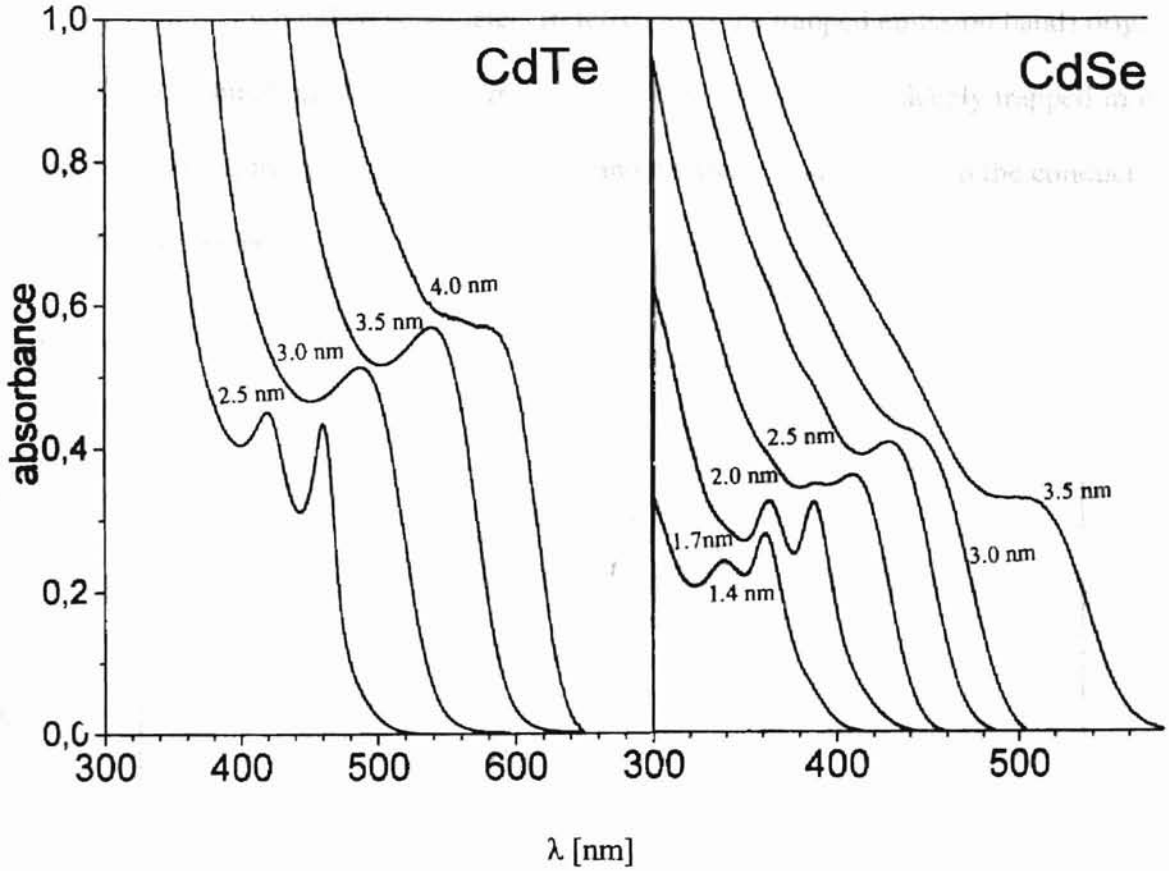

Fig. 4 UV-vis absorption of thioglycerol stabilized CdSe and CdTe nanoparticles
CdSe particle diameter: 1.4 nm ~ 3.5 nm; CdTe particle diameter: 2.5 nm ~ 4 nm

4. Photoluminescence (Fluorescence Emission). Most nanoparticle solutions, especially semiconductor nanoparticles are photoluminescent in red, yellow or green, depending on the size and electronic structure. The electronic structure of semiconductor nanoparticles differs from that of the bulk[39]. Most often, two kinds of excited states above the valence band of semiconductor clusters are considered: excitonic states (the energy levels associated with the core and positioned right below the valance band) and surface traps (surface state energy levels come from the surface defects). In Fig.5, the sharp band near the peak maxima of UV absorption at higher energy (referred to as excitonic emission band) corresponds to the

radiation from the core energy level to the valence band of the nanoparticles. The broad band covering almost two hundred nanometers (referred to as the trapped emission band) origins from the recombination of charge carriers (i.e.. electrons and holes) deeply trapped in the imperfect surface, formed by the edge atoms and believed to shift closer to the conduction band at lower temperature.

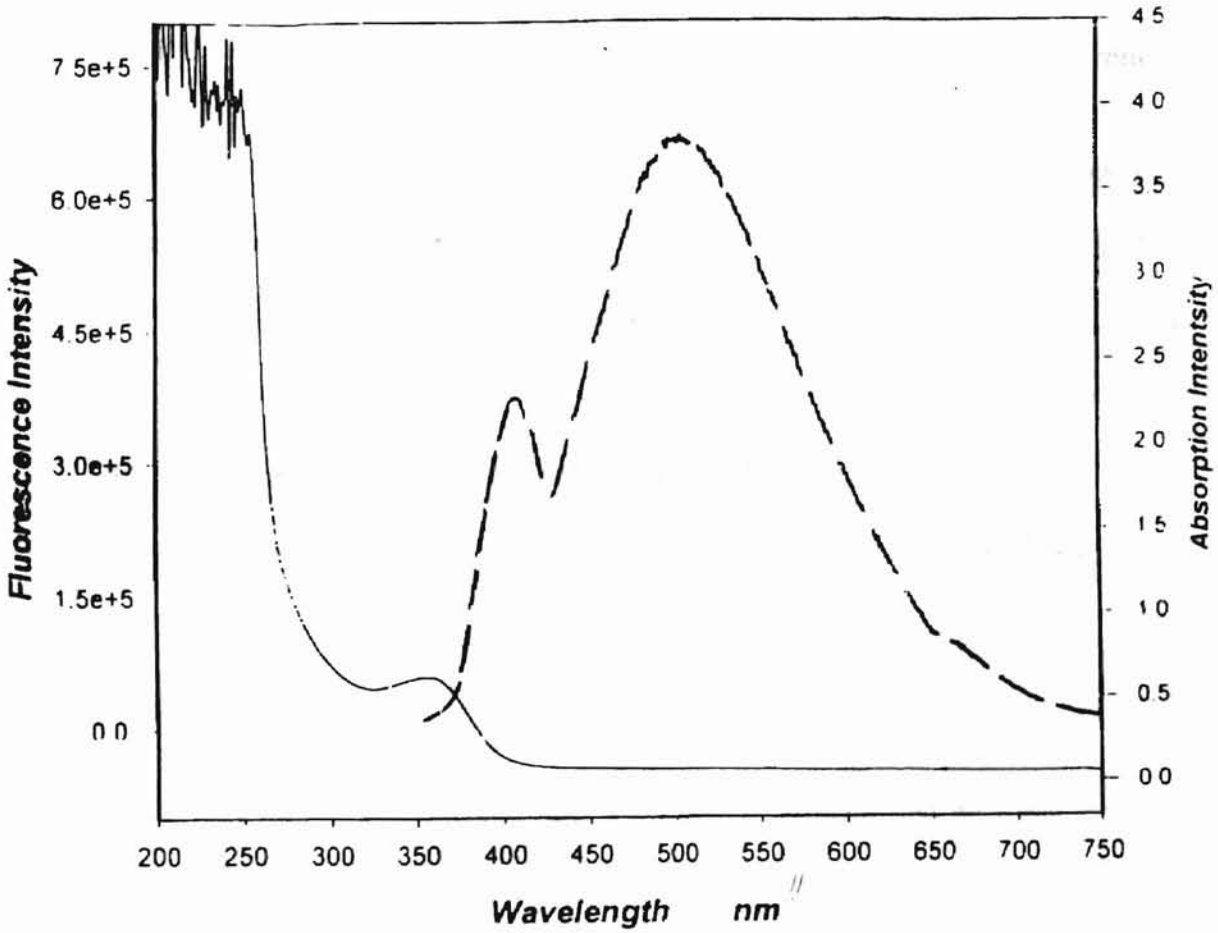

Fig.5. Fluorescence emission and UV adsorption of CdS nanoparticles stabilized by ethyl-hexanoate and DMSO

The existence of the trapped emission band decreases the quantum yield of the excitonic luminescence. Which of the two bands dominates in emission is a case by case issue. The

emission band often becomes weaker with time or increasing temperature. Typically, in the trapped band, the low energy side decays slower than the peak and the high energy side, in other words, shorter lived states tend to emit at higher energy. The quantum size effect appears to be less obvious in the trapped emission band than in the excitonic band[40]. Another useful technique in photoluminescence is the acquisition of the excitation spectra. When obtained at various emission wavelengths, such spectra reveal the number of emissive species[16]. The profile of the excitation spectra should resemble that of the UV absorption.

5. NMR. ^{1}H, ^{13}C, ^{31}P NMR and solid state[41] ^{1}H, ^{13}C NMR of organic capping agents have been successfully used to investigate the surface structure of semiconductor nanoparticles[42,43]. In general, homogeneous broadening[44] of the lines can be observed in NMR spectra of the molecules bonded to or absorbed on the surface of nanoparticles. The broadening is rationalized as slowing down of the molecule tumbling motion at surface, low motional average and fast T_2 relaxation[45, 46] which approach the T_2 times in solid state NMR. Thus, NMR can distinguish the surface-attached molecules from the free solution molecules unless the surface attached-molecular become NMR silent.

Surface coverage of the organic molecules then could be quantified by comparing the integrated signal of the stabilizers with that of an internal standard at known concentration, assuming the particle surface as a completed shell. The broadening effect and chemical shift may or may not be dependent upon the particle size, which is determined by the nature of the capping agent. In case of an aromatic stabilizer such as thiophenol, the C_6 ring can only be oriented perpendicular to the surface. As the size decreases, the surface area and surface coverage increases. The ring molecules experience more stereo hindrance and faster T_2

relaxation. As a result, the broadening effect is more obvious as the size decreases (Fig.6). While in the case of a chain stabilizer such as thioglycerol, the molecule has two more functional groups other than the thio which could be also bound to the surface. The molecule is believed to wrap around the surface of the particle and has very little mobility and little motional average (Fig.7). The dependence of broadening on the size seems less significant.

^{113}Cd resonance could be very weak in intensity but is more straightforward. The capped surface Cd could be clearly distinguished from the uncapped surface and the core Cadmium atoms[47], from which the number of surface atoms and organic molecule coverage could be easily obtained through integration.

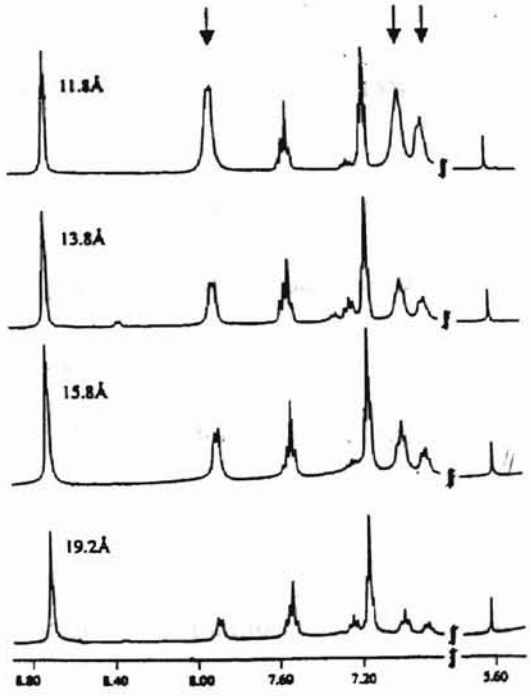

Fig. 6 ^{1}H NMR of thiophenol adsorbed at CdS nanoparticle surface with different particle radius ranging from 11.8 Å to 19.2 Å

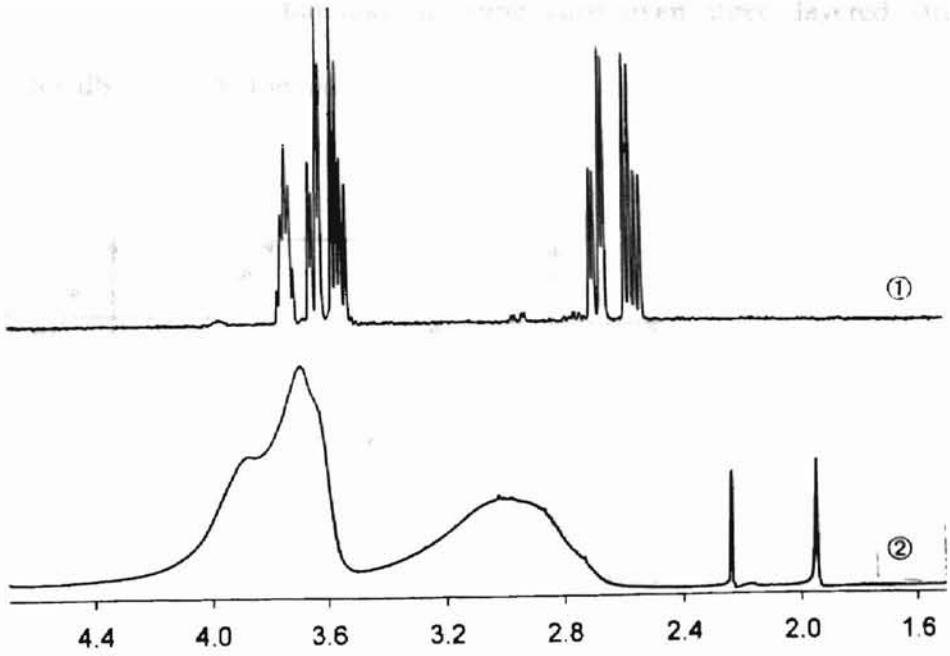

Fig. 7 ^{1}H NMR of free and adsorbed thioglycerol on CdS nanoparticle surface. 1). Free thioglycerol in the solution; 2). Adsorbed thioglycerol on CdS nanoparticle surface

E. SURFACE MODIFICATION OF SEMICONDUCTOR NANOPARTICLES

Semiconductor nanoparticles have many possible applications. But most of them are not very stable, especially as the particle size decreases. Surface modification could not only improve the material stability but also the performance in many applications. Moreover, the modification could provide a pathway to biologically, catalytically, electronically and optically tunable nanoparticles.

Most generally, the surface modification is accomplished by coating the semiconductor nanoparticles with a monolayer of organic or inorganic material: 1). Inorganic compounds. A different layer of semiconductor material can be deposited on nanoparticles: CdS/HgS, HgS/CdS, CdS/ZnS, ZnSe/CdSe, TiO_2/SnO_2, Fe_2O_3/CaO, etc.. Coating has been investigated

in which core-shell structure-and in some case even three layered structure like CdS/HgS/CdS -could be formed.

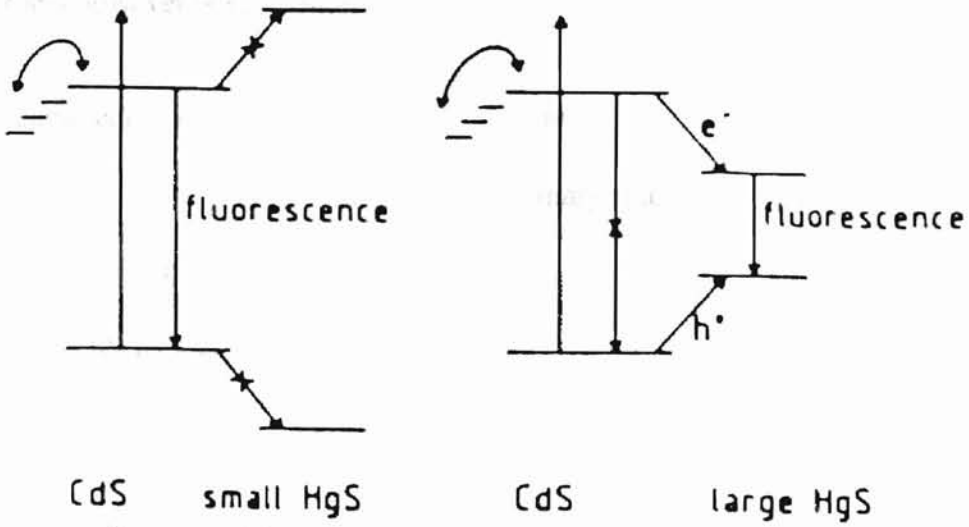

Fig.8 Energy scheme of CdS/HgS core shell nanocrystalline
core-CdS, shell-HgS

The growth of one semiconductor material on the other one is determined by matching the crystal lattice constants of the core and the shell. Inorganic coating has a strong impact on the optical properties of the nanoparticles. It was noticed that the character of emission of the core-shell structure varies with the band gap energy (E_g) of the overlayer[48-57]. Coating a semiconductor nanoparticles with one which has a larger E_g relative to the core typically results in the enhancement of nanoparticles emission due to the retardation of non radiation recombination mediated by surface states, while a layer of a smaller E_g semiconductor provides additional area of delocalization for electrons and holes accompanied by a red shift of emission (Fig.8). Core-shell structure may enhance the solubility, photostability of

nanoparticles, induce new emitting bands, and may also enhance the quantum yield of the excitonic emission by blocking the surface traps, and increase the selectivity, efficiency of light-induced reactions occurring on the surface[58, 59]. The shift in optical absorption spectrums however is very small.

2). Organic compounds: glycerols, thiols, polyphosphate, alkylphosphine oxide and other stabilizers or competitive exchanges of the primary stabilizing molecules [60, 61] with Lewis base character can be used to covalently bond to the metal site (Lewis acid sites) on the semiconductor nanoparticle surface.

The extent of interaction between HOMO and LUMO of these modifiers with VB (valence band) and CB (conduction band) is negligible. This type of modification does not demonstrate luminescence effects other than an alteration of the rate of the surface non radiative recombination and/or luminescence quenching. The stability of particles could be increased and the formation of larger agglomeration could be effectively eliminated. By exchanging the surface organic molecules, surface charge, surface polarity, solubility, quantum yields of the emission peaks could also be changed.

3). Metal ions. Ions can be doped into the crystal lattice of the metal sulfide nanoparticles or attached to the surface and form a discreet M-S shell. In Cu^+ doped ZnS system, Cu^+ replaces the Zn^{2+} ion in the crystal lattice. New emission bands are observed at different dopant concentrations[62, 63] which are attributed to the dopant center.

CHAPTER II

SYNTHESIS OF CdS, CdSe NANOPARTICLES, CuBM COMPLEX AND THEIR SPECTROSCOPIC CHARACTERIZATION

A. MATERIALS

$Cd(AC)_2 \cdot 2H_2O$ (Aldrich), $Cd(ClO_4)_2 \cdot 4H_2O$ (Aldrich), sodium citrate ($Na_3C_6H_5O_7 \cdot 2H_2O$) (EM Science), bipyridine-dichloroplatinum (Aldrich), thioglycerol (Aldrich), bipyridine-dichloropalladium (Aldrich), thiourea (Aldrich), thioacetamide (Aldrich), N,N-dimethyl selenourea (Strem), mercurochrome (Aldrich), $CuCl_2 \cdot 2H_2O$ (Aldrich), Na_2S (Fluka), NaOH (EM Science), malonic acid $CH_2(CO_2H)_2$ (Aldrich), 2,2'-bipyridine (Sigma), rhodamine B (Fluka), basic copper carbonate [$CuCO_3.Cu(OH)_2$] (Aldrich), D_2O (99.9 atom % D, Aldrich), DMF (EM), acetone (Aldrich), dialysis membrane with MWCO of 15,000 (Spectra). All the chemicals are of A.C.S. reagent grade and were used as received without further purification. 18 MΩ water were used in all preparations.

B. PREPARATION OF CdS NANOPARTICLE STABILIZED BY THIOGLYCEROL; CdS, CdSe NANOPARTICLES STABILIZED BY SODIUM CITRATE AND METAL COMPLEXES

1. Synthesis of CdS nanoparticles stabilized by thioglycerol[68]

0.989 g $Cd(CH_3COO)_2 \cdot 2H_2O$ and 0.4 ml 1-thioglycerol were dissolved in 80 ml DMF and heated to 70°C under argon. 5 ml 0.4 g thiourea DMF solution was added to the mixture and the temperature was raised to 100°C. The mixture was then reflexed at 100 °C~105°C under

argon for 1~2 hours until the color changed to light yellow, cooled to room temperature, concentrated to 20 ml using rota-vapor. Acetone was added dropwise under vigorous stirring to the concentrated nanoparticle solution till it became cloudy. The precipitated large size nanoparticles were centrifuged out and washed with acetone. This procedure was repeated until the appropriate size distribution was reached.

CdS nanoparticles stabilized by sodium citrate can be synthesized by using Na_2S as the sulfide source[64] which is rapidly mixed with $Cd(ClO_4)_2$ at room temperature. The UV absorption of the CdS particles obtained from this method has no distinguishable absorption peak or shoulder due to very wide size distribution which is not suitable for our study. Generally speaking, if no size control procedure is used, the size distribution will depend on the concentration of the two ions and most importantly, on the rate of mixing of these two ions. Basically, the lower the concentration and the faster the mixing rate, the narrower the size distribution will be.

In our study, a new method using base-catalyzed hydrolysis of thioacetamide aided with the energy provided by microwave in the presence of $Cd(ClO_4)_2$ and stabilizer-sodium citrate was applied to obtain rapid and uniform formation of CdS nanoparticles with high stability.

2. Synthesis of CdS nanoparticles stabilized by sodium citrate (Abr. as CdS-citrate)

In 45 ml 18 MΩ water, 2.5 ml of 8 mM aqueous solution of thioacetamide and 0.025 g sodium citrate were mixed. To this, 2 ml of $1*10^{-2}$ M aqueous solution of $Cd(ClO_4)_2$ was added and the pH was adjusted to 9.2 by addition of 0.1 M NaOH. The solution was heated in a 1000 W microwave (Sharp) for 55 seconds. A yellow color solution was obtained and

dialyzed against sodium citrate solution and stored in dark. Different sizes of CdS nanoparticles were obtained by increasing the concentration of Cd^{2+} to $2*10^{-2}$ M, $4*10^{-2}$ M and $6*10^{-2}$ M with the particle diameter increased from 26 to30, 35 and 44 Å (Fig. 9). Higher pH tends to give smaller nanoparticles but are featured by longer tails in UV-vis spectrum. No significant change in size was observed at even higher Cd^{2+} concentration.

3. Synthesis of CdSe nanoparticles stabilized by sodium citrate (Abr. as CdSe-citrate)

In 45 ml DI water, 2 ml of $1*10^{-2}$ M aqueous solution of $Cd(ClO_4)_2$ and 0.05 g sodium citrate were mixed. To this, 2 ml of 0.01 M freshly made aqueous solution of N,N-dimethylselenourea was added under degassing and then the pH was adjusted to 9.2 by addition of 0.1 M NaOH. The solution was heated in a 1000 W (Sharp) microwave for 50 seconds. A light red solution was obtained and dialyzed against sodium citrate and $Cd(ClO_4)_2$ solution. Different sizes of CdSe nanoparticles were obtained by increasing the concentration of Cd^{2+} to $2*10^{-2}$ M, $4*10^{-2}$ M and $6*10^{-2}$ M, $8*10^{-2}$ M, $10*10^{-2}$ M, $20*10^{-2}$ M, $30*10^{-2}$ M, with the particle diameter increased from 22 Å to 24, 26, 28, 30, 34, 40 and 46 Å (Fig. 9), while the concentration of selenourea and pH remained the same and sodium citrate was increased from 0.05 g to 0.075 g for Cd^{2+} at $8*10^{-2}$ M, $10*10^{-2}$ M and to 1.00 g for Cd^{2+} at $20*10^{-2}$ M, $30*10^{-2}$ M. No significant change in size was observed at even higher Cd^{2+} concentration. Thus prepared CdSe nanoparticle aqueous solutions did not precipitate for at least two weeks in the refrigerator. Additional increase of pH resulted in even smaller size of CdSe nanoparticles (10 nm decrease in UV-vis absorption could be observed at pH 9.5 with same Cd/S ratio) with lower stability.

4. Synthesis of (2,2'-bipyridyl-N,N')(malonato-O,O')-copper(II) Monohydrate (Abr. as CuBM)[65]

177 mg [$CuCO_3.Cu(OH)_2$] (0.79 mmol.), 43 mg Na(OH) (0.9 mmol.), 83 mg malonic acid (0.79 mmol.) and 124 mg 2,2'-bipyridine (0.79 mmol.) were mixed in 40 ml distilled water and reflexed for 3 hours. The solution was concentrated in a rotatory evaporator until small crystals appeared. Then, the reaction vessel was cooled and the solid was allowed to precipitate. The blue crystalline product was washed 3 times in acetone followed by drying in vacuum. Yield 48.3%.

5. Synthesis of Ru(2,2'-bipyridyl-N,N')$_2$Cl$_2$[66], Fe(2,2'-bipyridyl-N,N')Cl$_2$ and Fe(2,2'-bipyridyl-N,N')$_3$Cl$_2$[67]

Ru(2,2'-bipyridyl-N,N')$_2$Cl$_2$: 1.37 g $RuCl_3 \cdot 7H_2O$, 1.56 g 2,2'-bipyridine and 1.4 g LiCl was mixed together in 8.5 ml DMF in a 3-neck flask. The reaction mixture was then reflexed for 8 hours before 50 ml acetone was added and cooled to room temperature. The solution was stored at 0°C overnight and the black tinny crystal was filtered out by a crucible, washed with 5 ml 18 MΩ water 3 times followed by ethyl ether.

Fe(2,2'-bipyridyl-N,N')Cl$_2$ and Fe(2,2'-bipyridyl-N,N')$_3$Cl$_2$: 0.905 g Fe powders were added to 30 ml oxygen free HCl at 80°C under stirring in N_2 in a 3-neck flask. After all the Fe powder was dissolved, the temperature was raised to 100°C for HCl to evaporate under vigorous stirring in N_2. The temperature was allowed to drop to 60°C and 30 ml oxygen free absolute ethanol was added under stirring till all green color $FeCl_2$ was dissolved. The solution then was then divided into 25 ml solution (a) and 5 ml solution (b).

1. 30 ml 0.2 g 2,2'-bipyridine ethanol solution was added to solution (a) at 60°C under N_2 atmosphere drop by drop for about 10 minutes through a pressure balancing funnel. Maintaining N_2 atmosphere, the solution was stirred at 60°C for additional 5 minutes and stored at 0°C for overnight before yellow crystals were filtered out and washed with ethanol.

2. Solution (b) was added dropwise through a pressure balancing funnel to a 30 ml 1.54 g 2,2'-bipyridine ethanol solution under stirring in N_2 at room temperature. The solution was then stirred for additional 30 minutes before 120 ml ethyl ether was added. Stored the solution at 0°C for overnight and the orange color crystal was filtered out and washed with ethanol.

C. INSTRUMENTATION

1. NMR. ^{1}H NMR spectra were recorded on Inova 400 spectrometer using ID5 probe at room temperature. CdS stabilized by sodium citrate was synthesized in D_2O. Water suppression with zero spinning was used in all measurements. The spectrums were averaged over from 256 up to 2048 scans depending on signal intensity and S/N ratio. Water resonance peak in D_2O at 4.80 ppm was used as reference for all spectrums, no internal standard was added.

2. Fluorescence. All fluorescence spectra were recorded on Fluorolog-3, ISA. spectrophotofluorimeter, operating with a 450 W xenon arc lamp as a light source. The increment was set at 1 nm, integration time 0.4 s, signal S for emission measurements and S/R for excitation measurements. Slit width (expressed as band pass) varied from 2 to 10 nm according to the signal intensity and S/N ratio but remained the same for a batch of analysis. Optical filters were used to cut off Raman scattering light of water molecules. Excitation and

emission monochromators were calibrated before each series of measurements.

3. UV-vis. Optical absorption measurements were performed in water in 1~. 1 cm quartz cuvettes using a Hewlett-Packard 8453 diode array spectrophotometer in air under room temperature. Air was used as blank for compensation for all spectra while for rhodamine B absolute ethanol was used. Concentrations of CdS nanoparticles remained the same with those for fluorescence experiments.

4. Powdered X-Ray Diffraction. The XRD patterns were obtained with a Philips Analytical Diffractometer PW3710 , Cu Kα radiation operating at 40 kV tension and 45 mA current. The patterns were recorded over the 2θ range from 2.0 to 60 with a 2θ step of size of 0.02° and a scanning rate of 4 s per step. CdS nanoparticle powder was obtained by adjusting the pH of CdS nanoparticle aqueous solution to 4.6 after dialyzing exclusively against water for 12 hours. The precipitated CdS-citrate was centrifuged out, washed with water and dried in vacuum.

5. HREM: HREM samples were prepared on copper grids by floating the grid on the surface of aqueous nanoparticle solutions to assemble a thin discrete layer on the surface. Extra particles were washed off by floating the grid on the surface of water. All the pictures were taken on Phillips CM 300 instrument operating at 200 kV.

6. EPR. Electron paramagnetic resonance (EPR) measurements were performed on Bruker ER 200D SRC with the center of field set at 3280 G, sweep width 800 G, gain $8*10^4$, microwave frequency 9.78 GHz, microwave attenuation 22. Data of CuBM before and after modification to CdS particle surface was collected in a thin quartz cell.

7. XPS. All the measurements were taken on ESCALAB 250, VG Scientific instrument.

8. Time-resolved photoluminescence. Time-resolved photoluminescence (TRPL) measurements were carried out using a tunable picosecond pulsed laser system consisting of a cavity-dumped dye laser synchronously pumped by a frequency-doubled mode-locked Nd:YAG laser as an excitation source and a streak camera for detection. The output laser pulses from the dye laser had a duration of less than 5 ps and were frequency doubled into the ultraviolet spectral region by a nonlinear crystal. Samples for TRPL measurements were prepared the same as for light induced modification studies.

D. CHARACTERIZATION OF CDS, CDSE NANOPARTICLES

1. UV-vis absorption. The UV absorption spectrum CdSe, CdS semiconductor nanoparticles of different size obtained through synthesis methods 1) and 2) are presented in Fig.9 and Fig.10. The UV absorption maxima can be converted to the size of particles regardless of the type of the stabilizers unless the lattice patterns for the particles made following different procedures are different.

The XRD spectrum (Fig.13) of CdS-citrate indicates that CdS-citrate is crystalized in the cubic zinc blende structure, the size of CdS-citrate particles can be obtained empirically from the band gap energy/radius diagram (Fig.11) of CdS nanoparticles stabilized by thioglycerol[68], which are also in the cubic structure. CdSe particles are always found to be in the hexagonal wurtzite lattice. The radius of CdSe-citrate particles could be obtained from the similar diagram of CdSe stabilized by TOPO[69] (Fig.12). As the size decreases, the absorption maxima blue shifts to higher energy for both CdS and CdSe particles, while the

extinction coefficient increases (known as the quantum size effect). The diameter of CdSe nanoparticles in the citrate synthesis can be varied from 2.2 to 4.6 nm corresponding to the absorption maxima from 498 nm to 600 nm, while the diameter for CdS-citrate can be varied from 2.6 to 4.4 nm corresponding to the absorption maxima from 395 nm to 445 nm, with an error of ∓10Å. TEM images confirm the assessment yielding the range of diameters from 2 nm to 4 nm and the distribution of 15%.

2. Photoluminescence. The emission spectrum of CdSe-citrate and CdS-citrate are shown in Fig.14 and Fig.15. Concentration of CdS-citrate and CdSe-citrate nanoparticles was estimated to be 0.2 mM in the terms of Cd^{2+}.

Calculation from Table 1) and 2) shows that band gap of CdS (2.8 ev ~ 3.1 ev) is larger than that of CdSe (2.1 ev ~ 2.5 ev). Comparing the emission spectra of these two kinds of quantum dots, it can be noticed that the quantum yield of trapped emission bands of CdSe is much lower than that of the excitonic band while in CdS case, the excitonic band is much lower than the trapped band. This indicates that the energy level distribution differs between the two particles. In particularly, CdS nanoparticles should have greater density of intra band gap states, which facilitates nonradiation recombination of electrons and holes leading to weaker emission intensity.

The quantum size effect is obvious in the excitonic bands for both CdS and CdSe, while the trapped emission bands are not so sensitive toward size changes, being located in 600 nm region for both CdS and CdSe nanoparticles. The quantum yields for both excitonic and trapped emission increases as the particle size decreases. Calculations for CdS particles compared with the integrated emission of rhodamine B show that the quantum yield for

excitonic bands is around 0.2% while the trapped emission band is around 7%.

The quantum yield for trapped emission decreases faster over time than excitonic bands. Emission of CdS-citrate after dialysis against citrate solution is shown in Fig.16. Compared with that before dialysis, the trapped emission bands show a red shift due to the change in the adsorption layer on the nanoparticle surface.

Emission at low temperature (77K) is shown in Fig.17. Note at low temperature, the trapped emission band shows a blue shift while the excitation band becomes hardly noticeable. The origin of these effect of low temperature is not completely understood. It may be speculated that formation of a solid state at 77 K stimulates self-quenching of the excitonic emission due to the proximity of the nanoparticles to each other. Dipole-dipole interactions of the excited and ground states facilitate excitation energy transfer resulting in greater population of the intraband states.

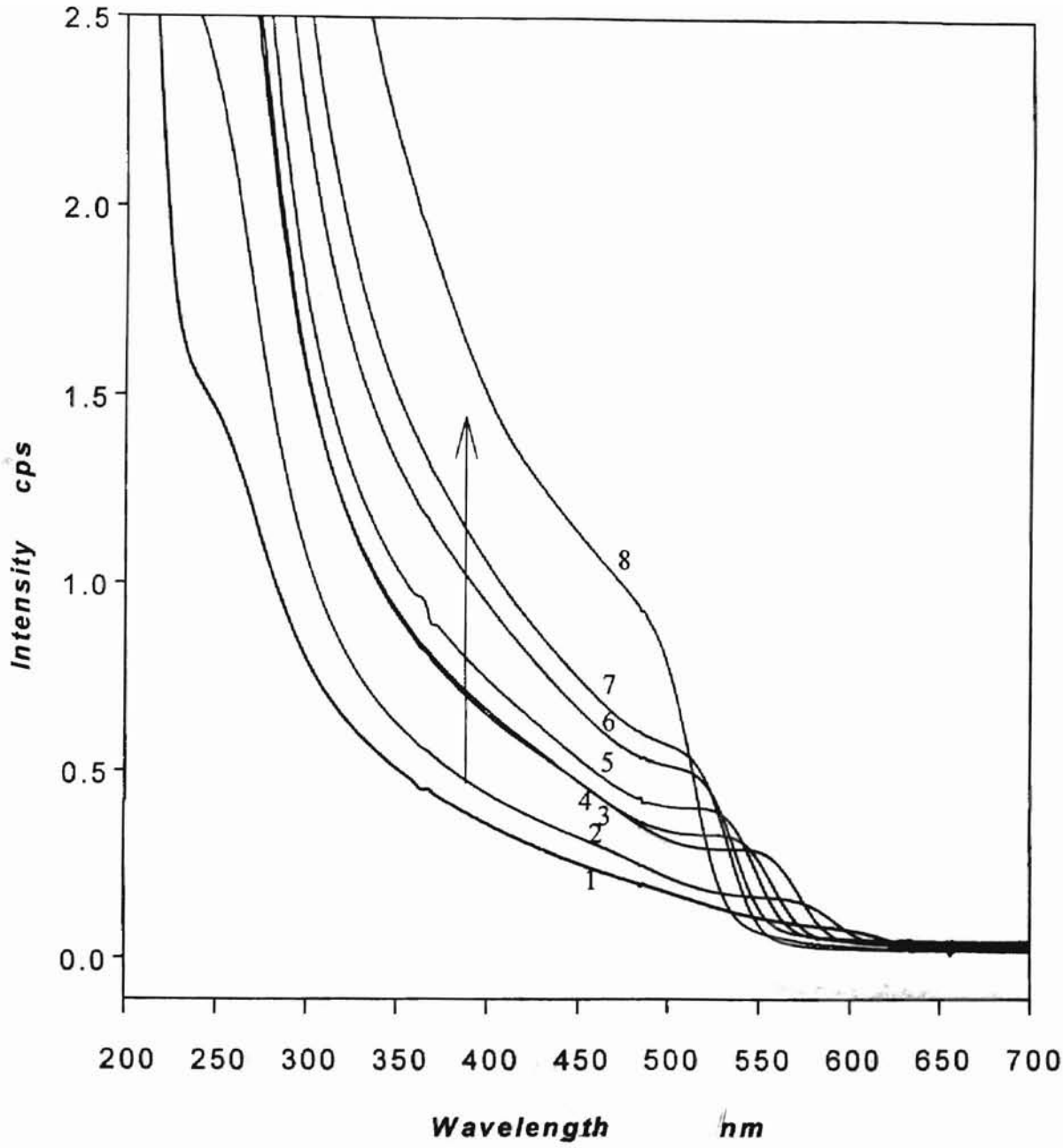

Fig.9. Optical absorption of different size CdSe nanoparticles stabilized by sodium citrate obtained through synthetic method 3. Concentration of CdSe-citrate nanoparticles was estimated to be 0.2 mM in the terms of Cd^{2+}. 1). Cd^{2+}/Se^{2-} = 1:1; 2).Cd^{2+}/Se^{2-} = 2:1; 3). Cd^{2+}/Se^{2-} = 4:1; 4). Cd^{2+}/Se^{2-} = 6:1; 5). Cd^{2+}/Se^{2-} = 8:1; 6). Cd^{2+}/Se^{2-} = 10:1; 7). Cd^{2+}/Se^{2-} = 20:1; 8).Cd^{2+}/Se^{2-} = 30:1

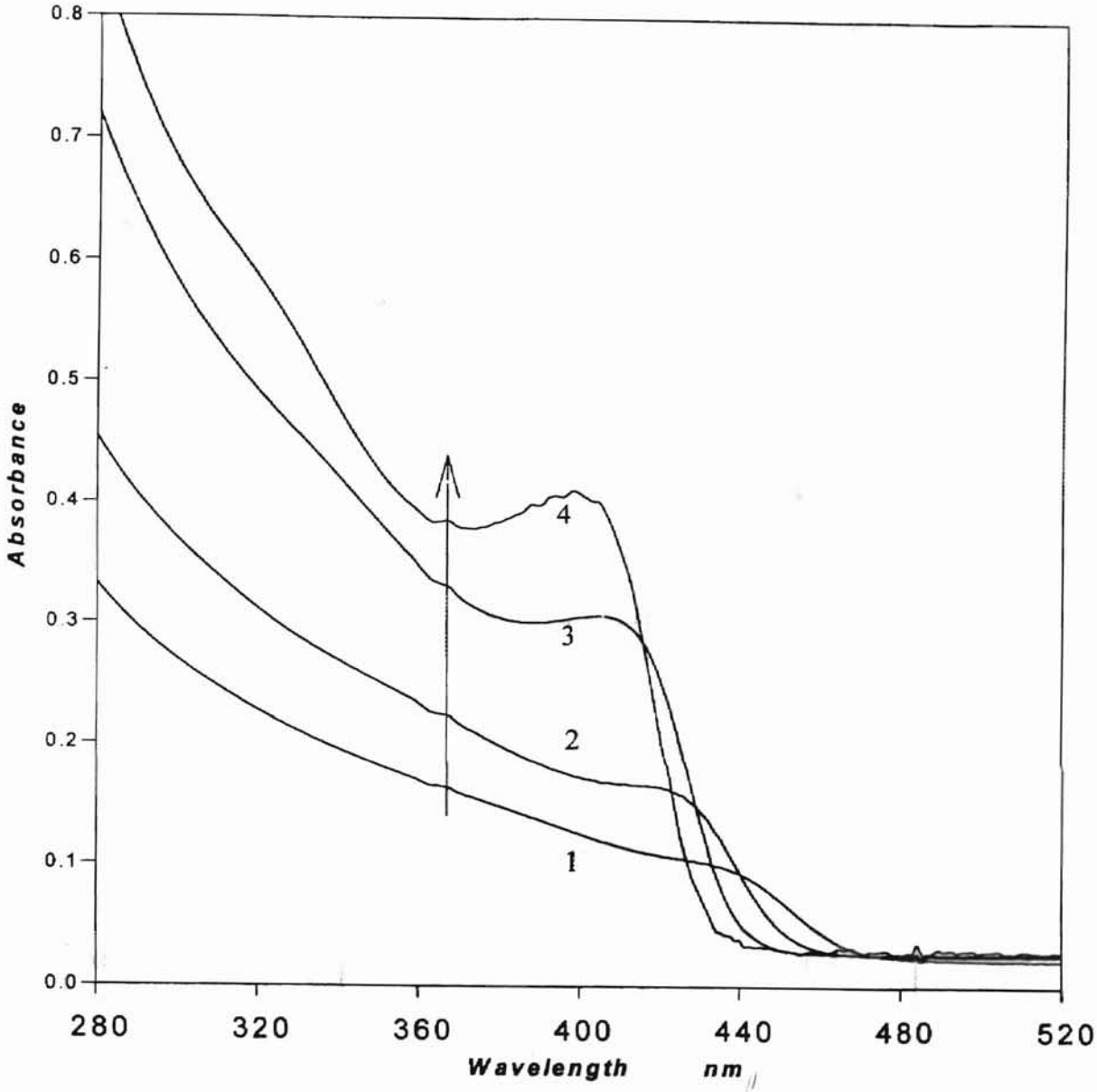

Fig. 10. Optical absorption of different size CdS nanoparticles stabilized by sodium citrate obtained through synthetic method 2. Concentration of CdS-citrate nanoparticles was estimated to be 0.2 mM in the terms of Cd^{2+}. 1). Cd^{2+}/S^{2-} = 1:1; 2). Cd^{2+}/S^{2-} = 2:1; 3). Cd^{2+}/S^{2-} = 4:1; 4). Cd^{2+}/S^{2-} = 6:1

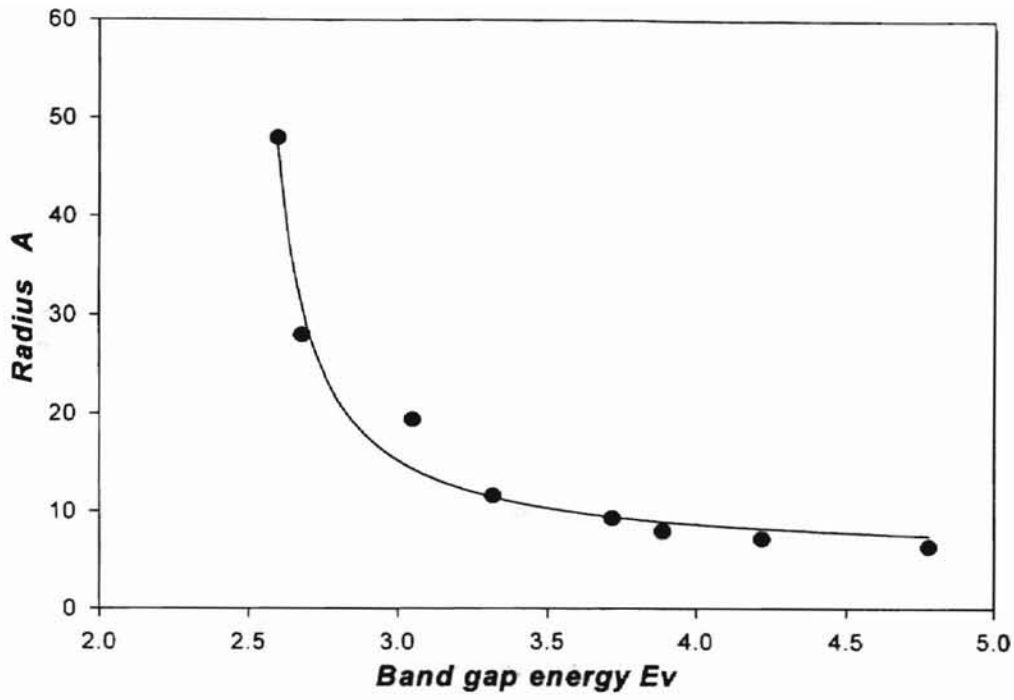

Fig.11 Band gap energy/size diagram of CdS nanoparticles stabilized by thioglycerol

Table 1. Particle radiuses of CdS-citrate measured empirically through Fig.11

Abp. of CdS (nm)	395	410	425	445
Energy (ev)*	3.14	3.03	2.92	2.79
Radius of CdS(Å)	13.13	14.69	17.03	21.91
Agglomeration No.**	180	260	400	840

*Energy (ev) = 1241.4/λ (nm)

**Agglomeration No.=$\rho(g/cm^3)4/3\pi r^3(cm^3)N/!44.47$ ($N=6.023*10^{23}$, $\rho=4.50_{cubic}$)

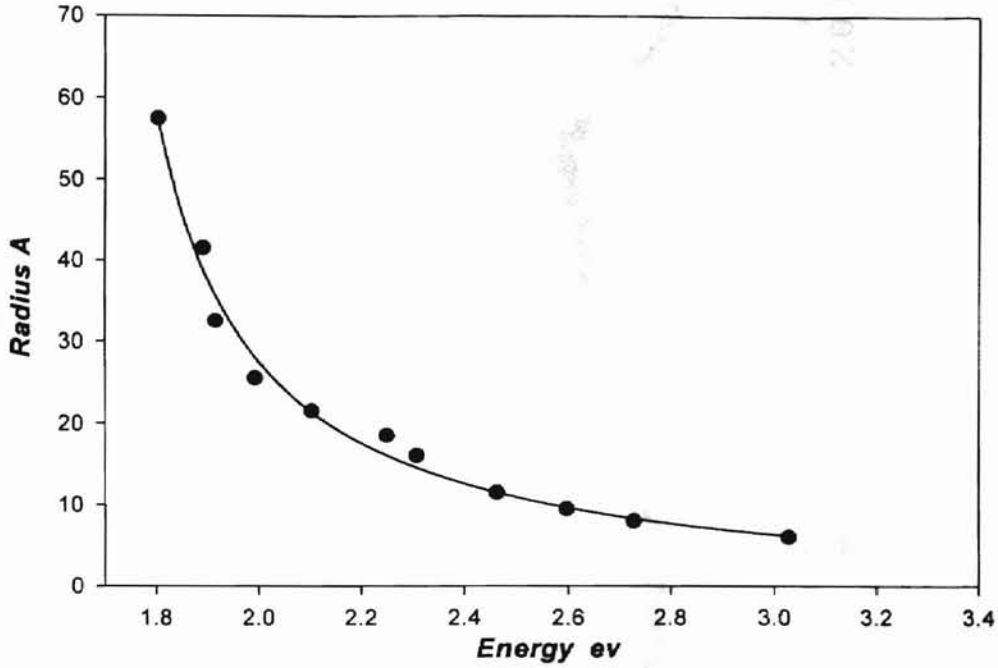

Fig.12 Band gap energy/size diagram of CdSe nanoparticles stabilized by TOPO

Table 2. Particle radiuses of CdSe-citrate measured empirically through Fig. 12

Abp. of CdS (nm)	600	580	560	545	535	524	512	498
Energy (ev)*	2.07	2.14	2.22	2.28	2.32	2.37	2.42	2.49
Radius (Å)	23.0	19.75	16.91	15.22	14.25	13.19	12.25	11.12
Agglomeration No.**	900	600	380	270	220	170	140	100

*Energy (ev) = 1241.4/λ (nm)

**Agglomeration No.=$\rho(g/cm^3)4/3\pi r^3(cm^3)N/191.36$ ($N=6.023*10^{23}$, $\rho=5.81$)

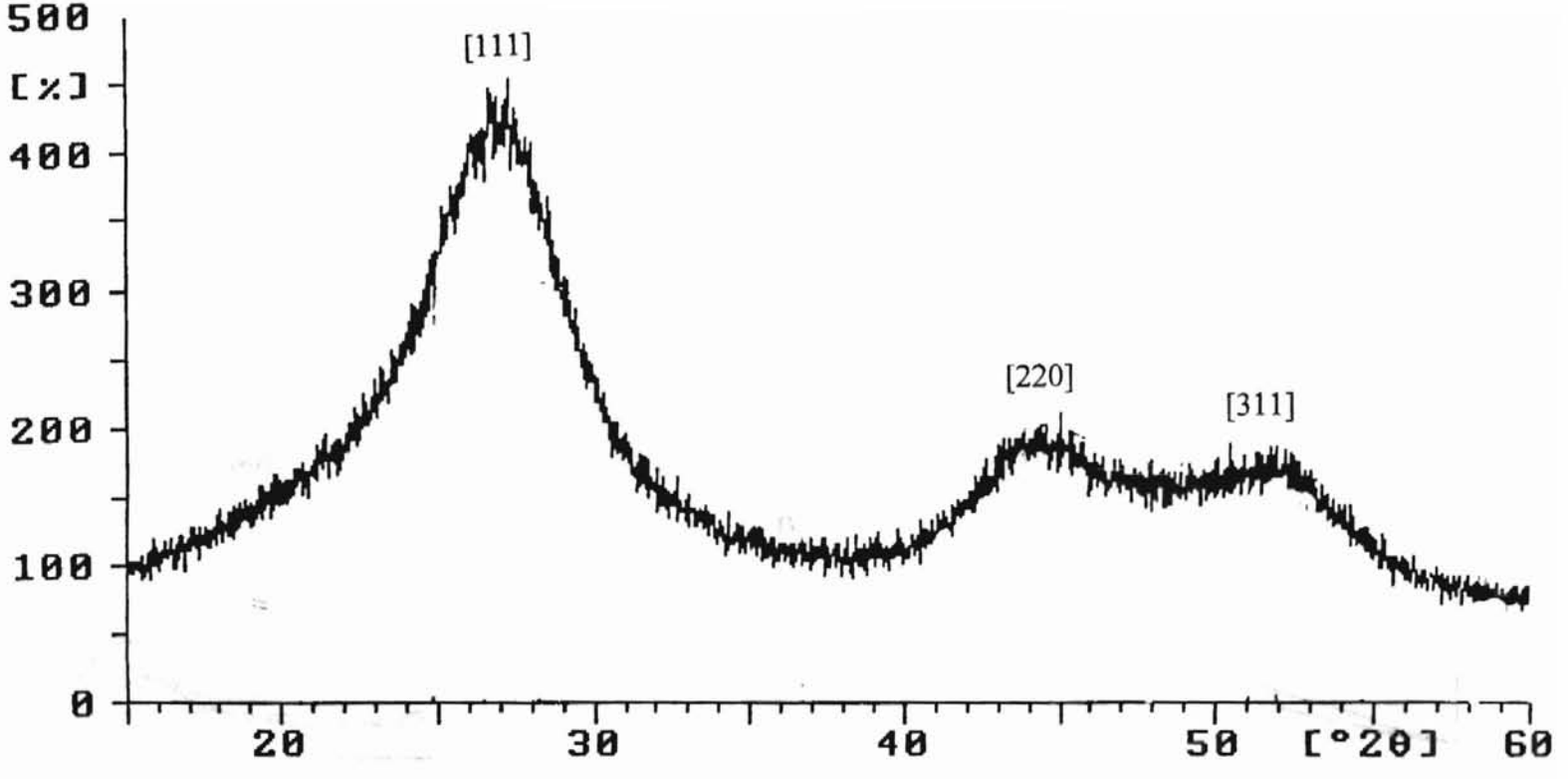

Fig. 13. XRD spectrum of CdS-citrate nanoparticle ins a powder form

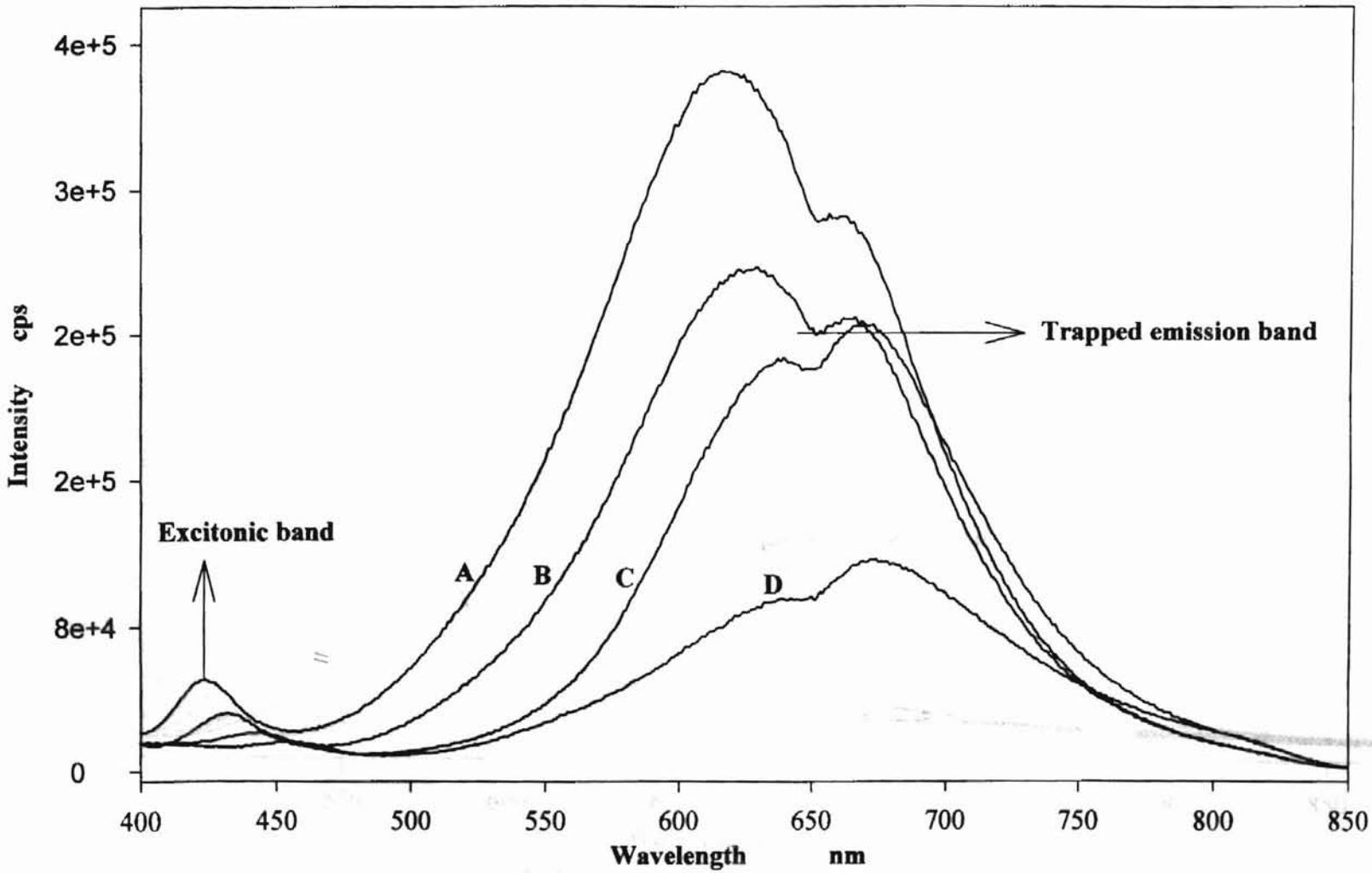

Fig. 14. Emission of CdS-citrate nanoparticles of various diameters

Diameter of sampla A: 2.6 nm; sample B: 3.0 nm sample C: 3.5 nm; sample D: 4.5 nm

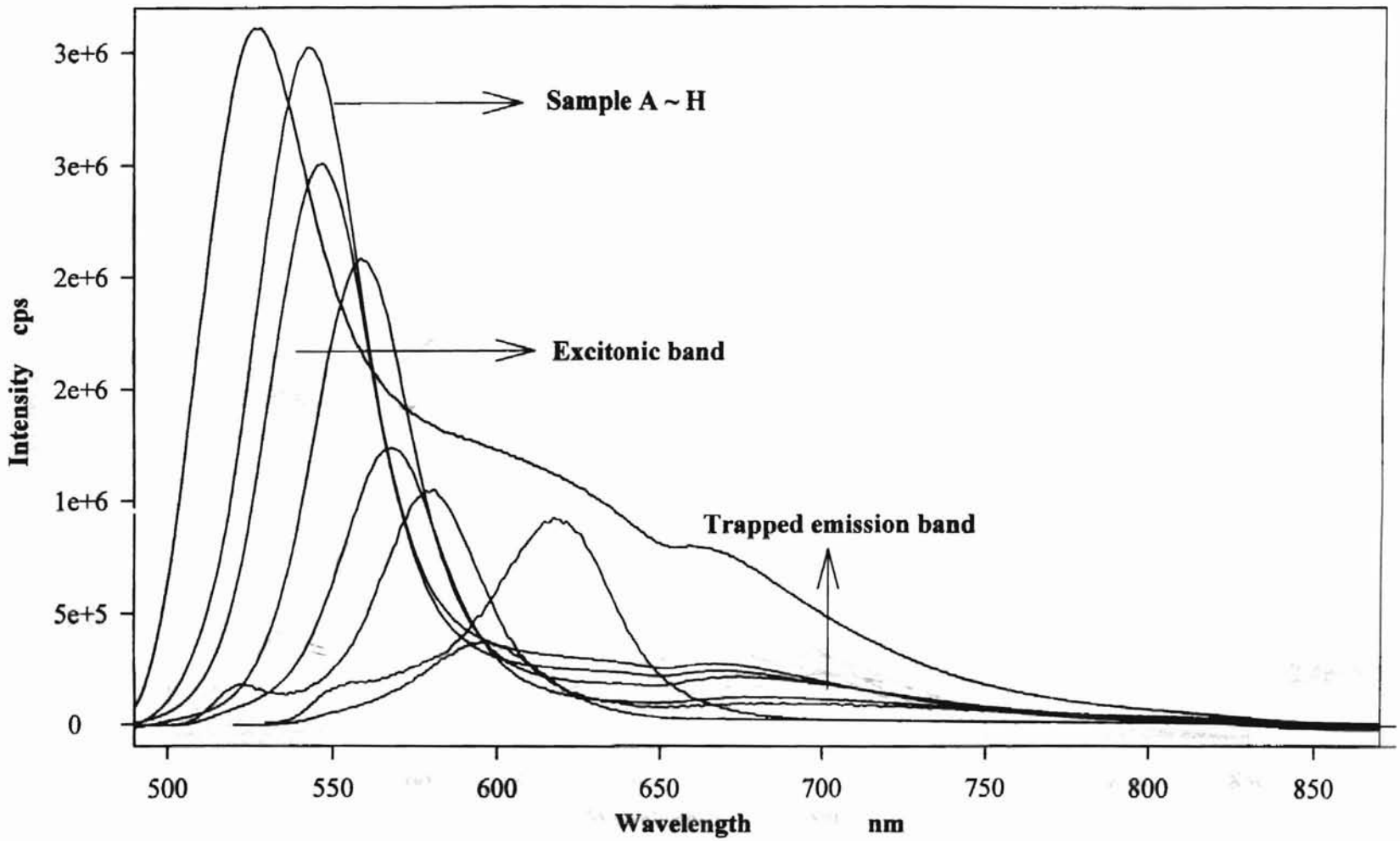

Fig. 15. Emission of various size CdSe-citrate nanoparticles

Diameter of sample A: 2.2 nm; sample B: 2.4 nm; sample C: 2.6 nm; sample D: 2.8 nm; sample E: 3.1 nm; sample F: 3.5 nm; sample G: 4.0 nm; sample H: 4.6 nm

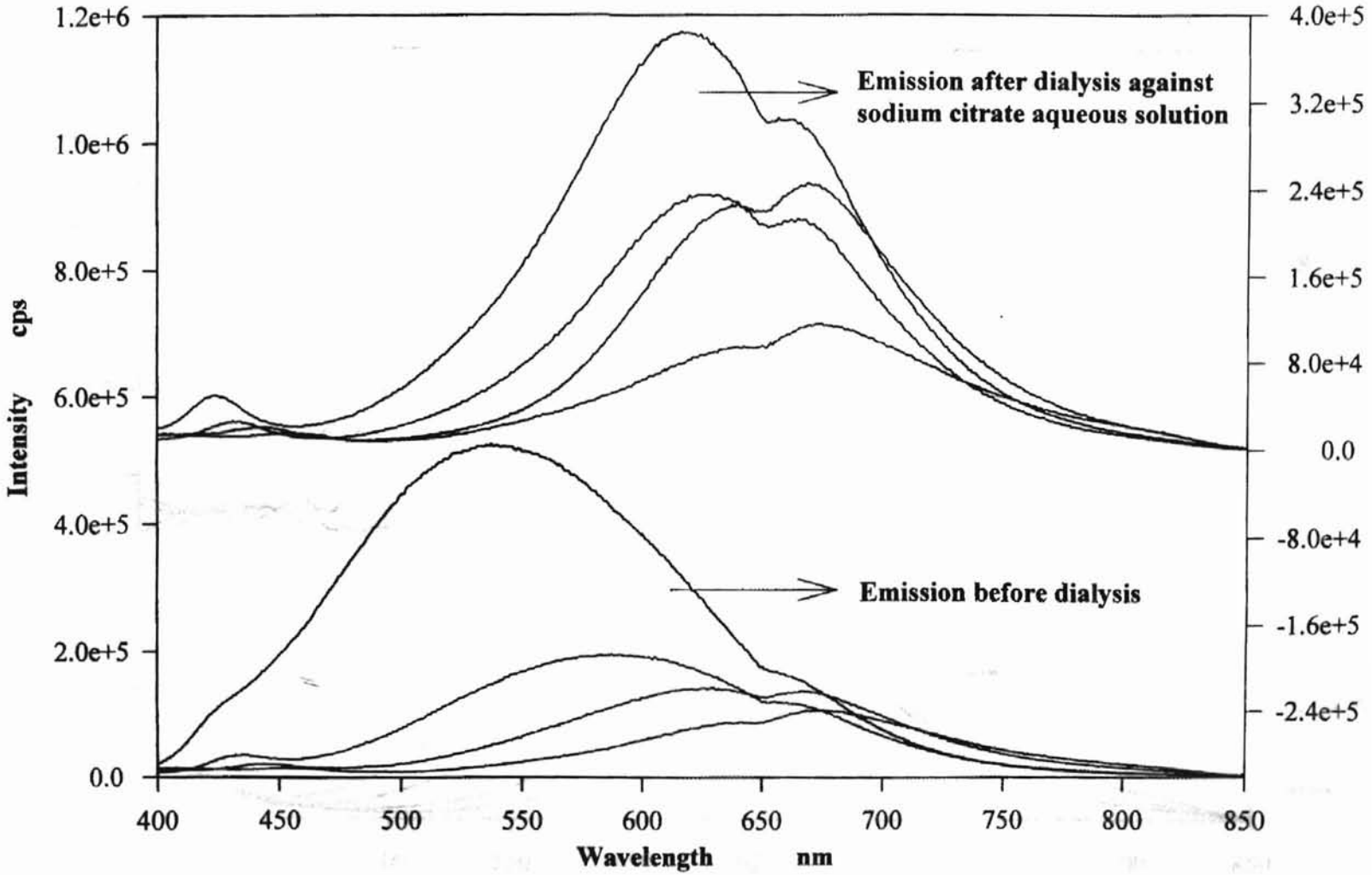

Fig. 16. Emission of CdS-citrate nanoparticles of various diameters before and after dialysis against citrate solution, pH of 9.1

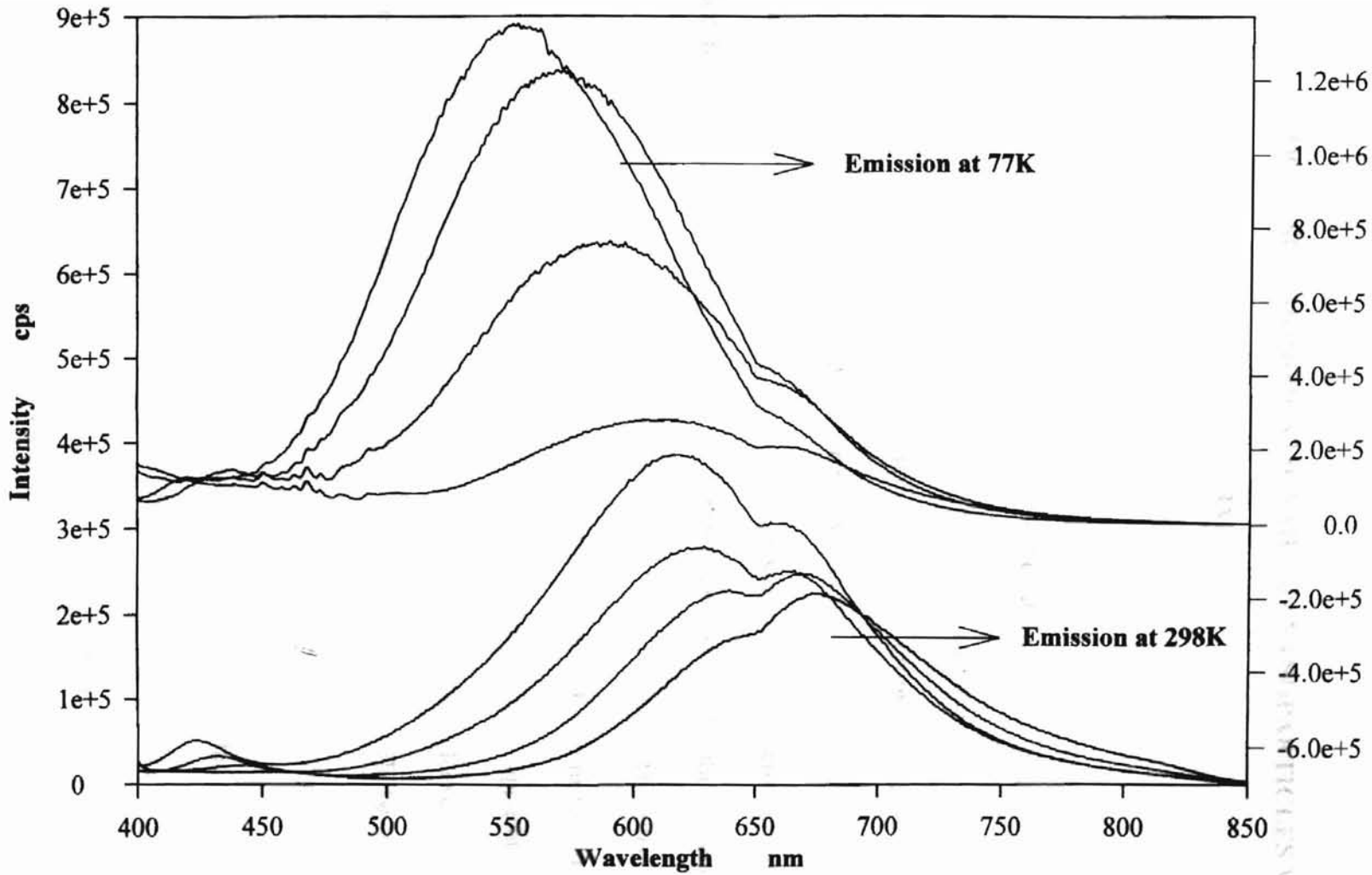

Fig. 17. Emission of CdS-citrate nanoparticles of various diameter at room temperature and 77 K

CHAPTER III

CHALCOGEN SITE MODIFICATION OF CdS NANOPARTICLES WITH CuBM

A. INTRODUCTION

Surface modification of nanoparticles can also be utilized to control the optical and electronic properties. Traditionally, the surface structure of semiconductor chalcogenide nanoparticles is chemically modified by binding organic groups to the metal sites. The method is quite straightforward due to the easy accessibility of the metal sites and the abundance of the electron rich organic modifiers such as amines, heterocyclic compounds and thiols acting as Lewis base. However, multiple studies showed that the core energy levels of the nanoparticles remain unaffected in the result of this derivation. The effect of surface modification to metal sites is limited to the alteration of the surface emission states which are poorly defined. Their optical properties are rarely considered for any applications because of the breadth of the emission band and high rate of thermal deexcitation. Surface modification that would affect the energy of the core states, will be of significant fundamental and practical importance.

As an alternative, to derivation of nanoparticle at metal sites the surface properties can be controlled by modification with Lewis acids by binding to the electron rich chalcogenide sites. Nanoparticles such as CdS, CdSe, PbS, ZnS, ZnSe may carry negative charges at the surface owing to the difference in the natural packing of crystal faces and various surface defects, which makes the chalcogen atoms located on the surface reactive with Lewis acids.

The choice of modification of nanoparticle to chalcogenide sites is based on the following considerations:

1). Surface chalcogen atoms are involved into both radiative and nonradiative processes in nanoparticles.

2). Lone pairs of surface chalcogen atoms are coupled to the internal energy states of nanoparticles.

3). Chalcogenide sites are known to be responsible for the oxidation of nanoparticles. Therefore, their modification can significantly reduce their deterioration.

Such modification involving organic groups is experimentally more challenging because organic Lewis acids are far less common. To choose the suitable modifier (metal complex) to couple with metal sulfide nanoparticles two major factors need to be taken into account:

1). The modifier should be a mild Lewis acid capable of binding to the surface sulfide ions yet does not react with stabilizers.

2). Aromatic groups should be present in the modifier in order to facilitate the interaction between the surface and core states of nanoparticle and electronic levels of the modifier.

Here we propose using mixed ligand metal complexes, with at least one labile inorganic ligand that can be easily replaced by S^{2-} groups on the surface of nanoparticles. The other ligands (strong bidentate agents such as bipyridine) will remain bound to the metal ion and will become a part of nanoparticle/metal complex supermolecule.

In this work, the modification of CdS semiconductor nanoparticle stabilized by sodium citrate through S sites was studied with a copper complex aqua(2',2'-bipyridyl-N,N')(malonato-O,O')-copper(II)monohydrate (CuBM) with the structure given at below. CuBM satisfies the criteria outlined above.

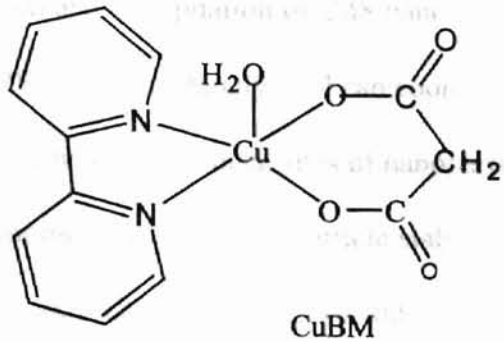

CuBM

Modification process is shown as scheme 3.

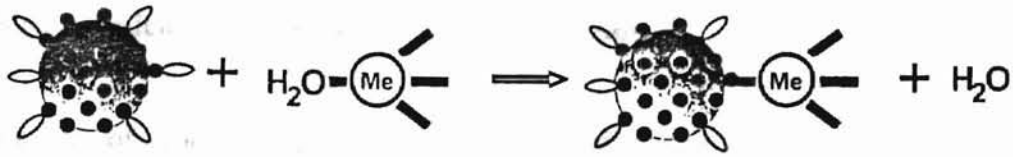

Scheme 3. Modification of CdS nanoparticles with metal complex

It is necessary to note that the complex and the type of nanoparticles were judiciously selected among many other possible candidates. As a part of this study, a new method of synthesis for nanoparticles utilizing citrate stabilizing agent had been developed. The need for this synthetic method originated in the fact that other stabilizers commonly used for synthesis of II-VI nanoparticles interfere with the modification by metal complexes.

Pt, Pd, Ru, Fe bipyridine complexes (synthesis and structure given in method 5, chapter II), mercurochrome (Hg aromatic salt) and CuBM as well have been used to modify CdS nanoparticles stabilized by thioglycerol, which resulted in either no noticeable coupling of

the two systems or a complicated coupling which may involve depletion of the surface thioglycerol molecules, leading to agglomeration and precipitation of CdS nanoparticles. The observations are attributed to the fact that RS^- groups of thioglycerol can coordinate to the metal complex modifiers and compete with the surface chalcogen sites of nanoparticles. To simplify the modification study, a convenient model of CdS nanoparticle stabilized by sodium citrate is chosen to be the focus of this research. Though citrate ion could be a mono-, bi- or even tridentata ligand binding to the nanoparticle surface depending on the pH as well as surface conditions, compared with S^{2-} ions, the complex of COO^- to Cu^{2+} is much weaker and therefore is less competitive especially in the presence of malonate, which has very similar coordination chemistry. At the same time, citrate ion is hydrophilic and makes the CdS nanoparticles highly soluble in aqueous solution.

The choice of copper complex for the surface modification was made because of the well-known copper ion doping of II-VI semiconductors. It results in appearance of new emission bands in the 400-600 nm region, which can be used for preparation of new light-emitting devices.

The objectives of this study were the following.

1). To develop a new technique of surface modification of nanoparticles and new synthetic pathways to optically and electronically tunable semiconductor supramolecules.

2). To determine the structure of nanoparticle/metal complex supramolecules.

3). To study the effect of surface modification to chalcogen sites on optical properties of nanoparticles.

B. RESULTS

1. Structure of CuBM modified CdS nanoparticles with

a. Optical absorption. Modification was achieved by mixing aqueous solution of CdS with that of CuBM at room temperature. CuBM concentration was set at 3.0 mM. The modification process monitored *in situ* by UV-vis absorption with Cu^{2+}:CdS particle (a synthetic ratio of Cd^{2+}:S^{2-}=4:1 was chosen) ratio of 60:1 for 16 minute time period is shown in Fig.18. Two isobestic points were formed on the spectrum, one from the absorption change of CuBM, the other from the change of CdS-citrate nanoparticles. As the CuBM double peak absorption band from 300 to 315 nm decreases, a new band around 277 nm increases, which indicates that the exchange of ligands occurs, *i.e.* the formation of Cu-S bound and the replacement of the hydrate. In the 400-480 nm region, a gradual broadening of the onset of CdS adsorption can be seen. An isobestic point forms as the CdS absorption maxima decreases and the absorption edge increase suggesting the alteration of the particle core states. Since no significant change in the size is found by TEM (Fig. 23), the red shift of the CdS band edge is, therefore, attributed to the perturbation of electronic levels of the core, possibly due to the expansion of the delocalization volume available for charge carriers of the CdS core. This indicates relaxation of size quantization effect in the modified nanoparticle.

UV absorption change of CdS in the presence of $CuCl_2$ is compared with that of CuBM, a little increase in the CdS absorption tail can be noticed (Fig.19). Since Cu_2S and CuS are less soluble than CdS, very small and discreet Cu_2S and CuS particles[70] could form on CdS

nanoparticle surface and influence the core energy through the lone pair on S^{2-}.

Different amounts of CuBM were used to modify the surface of CdS-citrate, with CuBM to CdS particle ratio equals to 20:1, 40:1, 80:1 as shown in Fig. 20. A new band appears around 277 nm in the copper complex absorption range and increases as the concentration of CuBM increases. The same increasing effect of CuBM concentration is obvious on the CdS nanoparticle absorption tail around 450 nm. By subtracting the absorption of CdS-citrate and CuBM from that of the modified CdS-citrate particles, a peak at 277 nm and a weaker one around 233 nm are revealed (Fig. 20 insert), indicating the formation of Cu-S bond and the restructuring of the copper coordination sphere. Both bands are attributed to the electronic transition in CuBM where the molecule of water is replaced with sulfur. Therefore, it would be important to compare the spectral changes in CuBM/CdS system with those in other ligand exchange reaction of CuBM.

The spectral signature of the reaction of Na_2S with CuBM is shown in Fig. 21. One can see that the MLCT bands of CuBM shift from 310 nm and 250 nm to 277 and 233 nm respectively. The consistent appearance of the band at 277 nm in CuBM/CdS and CuBM/Na_2S systems implies the formation of Cu-S bonds in both cases.

Dialysis against 18 MΩ water was carried out for the modified CdS nanoparticles (Fig.22) (4 ml of modified CdS-citrate solution against 1000 ml 18 MΩ water) after several hours when the solution of CdS-citrate and CuBM was mixed. Membrane with MWCO of 15,000 was used and total dialysis time was set as 12 hours, with the water changed every 6 hours. The UV absorption shows that after dialysis, a significant amount of CuBM remained attached to CdS-citrate nanoparticle surface.

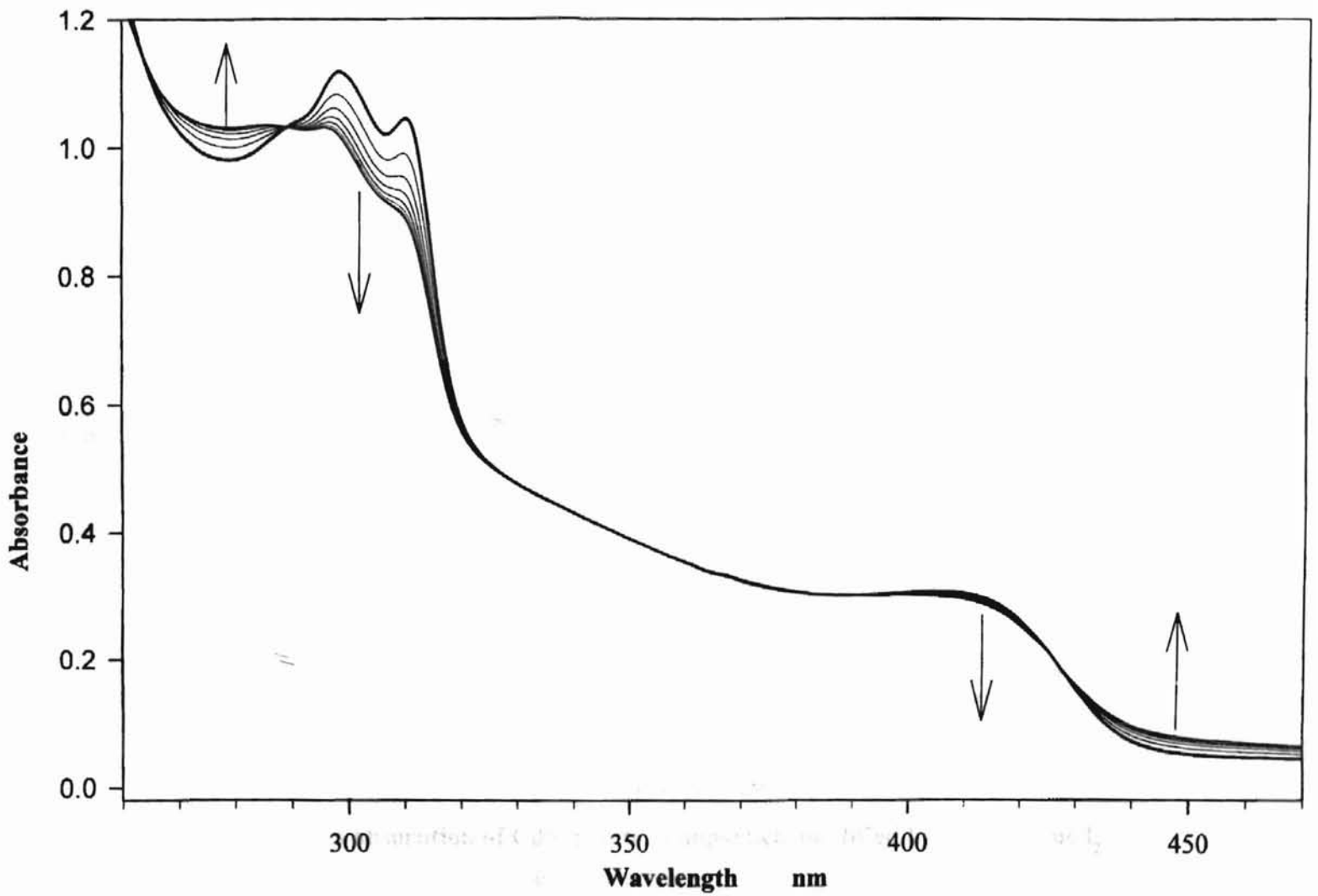

Fig. 18. In situ UV absorption monitoring of CdS-citrate/CuBM modification

CdS-citrate average diameter: 3.5 nm; CdS-citrate/CuBM 1:60, time interval 2 minutes

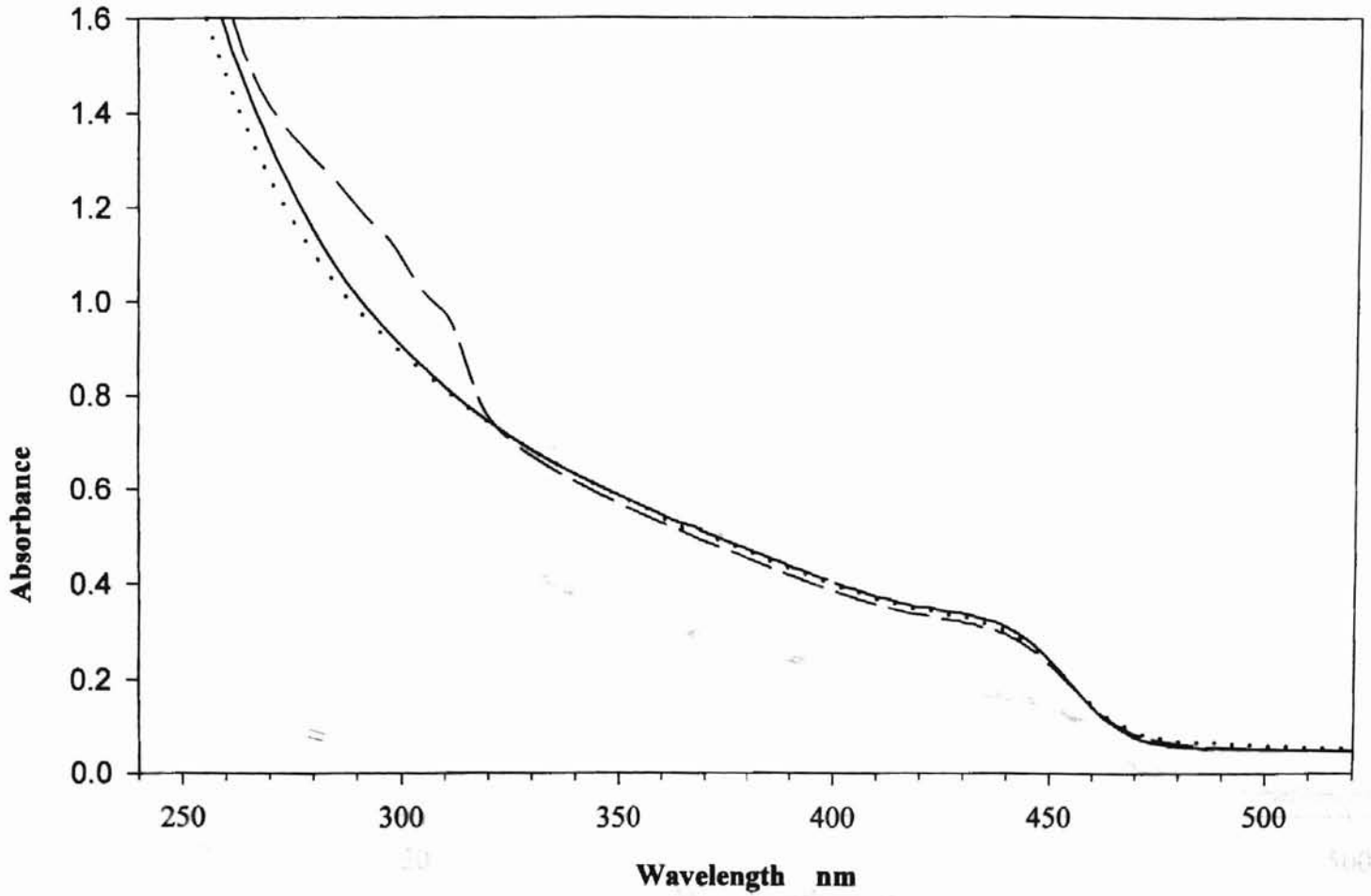

Fig. 19. UV-Vis absorption of CdS-citrate nanoparticle modified by CuBM, $CuCl_2$

__ Unmodified CdS-citrate nanoparticle

--- CdS-citrate in the presence of CuBM, CdS-citrate:CuBM = 1:60

.... CdS-citrate in the presence of $CuCl_2$, CdS-citrate:$CuCl_2$ = 1:60

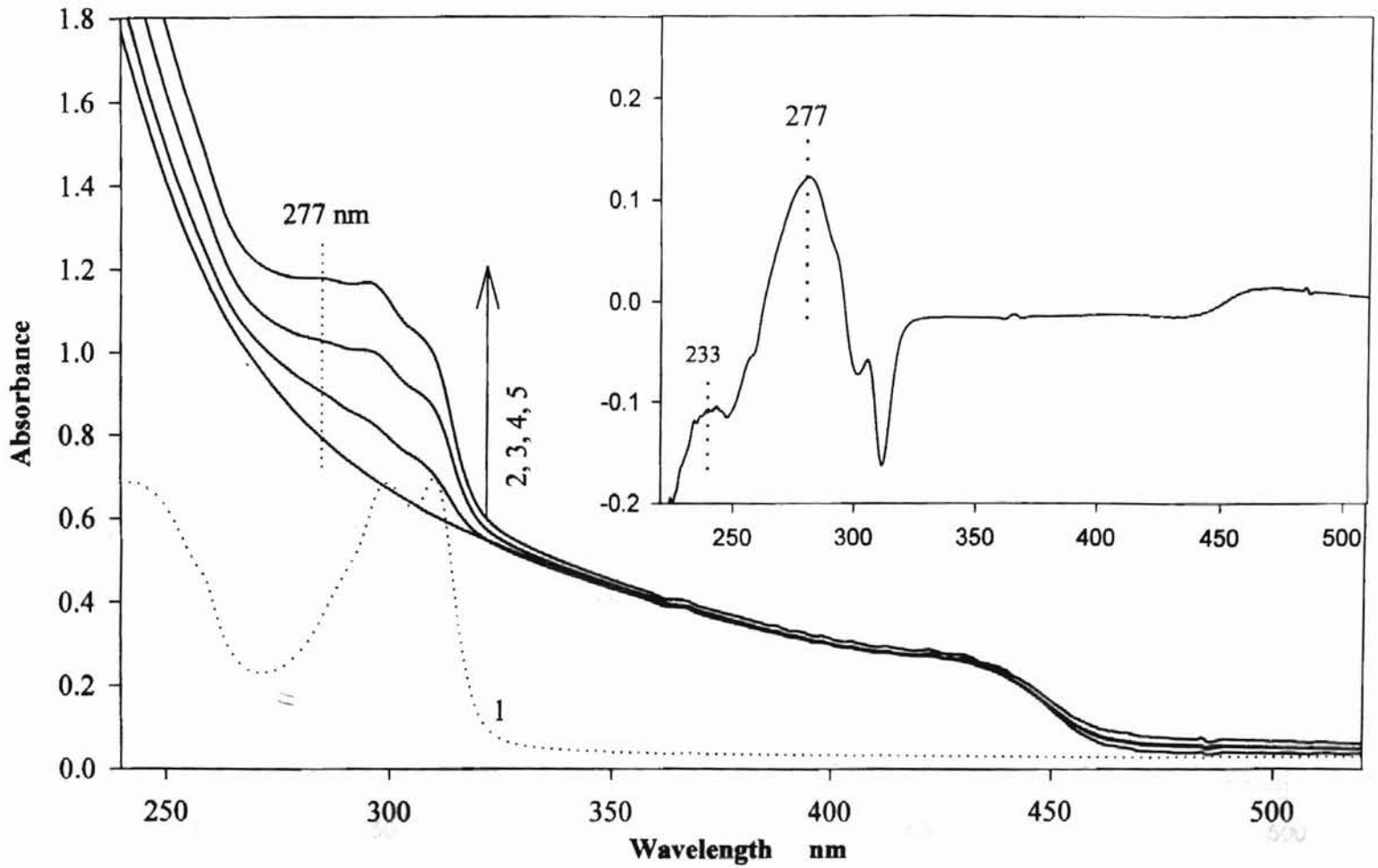

Fig. 20. Modification of CdS-citrate at different CuBM concentration

1. CuBM in aqueous solution; 2. CdS-citrate nanoparticle aqueous solution

3. 4. 5. CdS-citrate/CuBM = 1:20, 1:40, 1:80

Insertion: 5 subtract 2 and 1

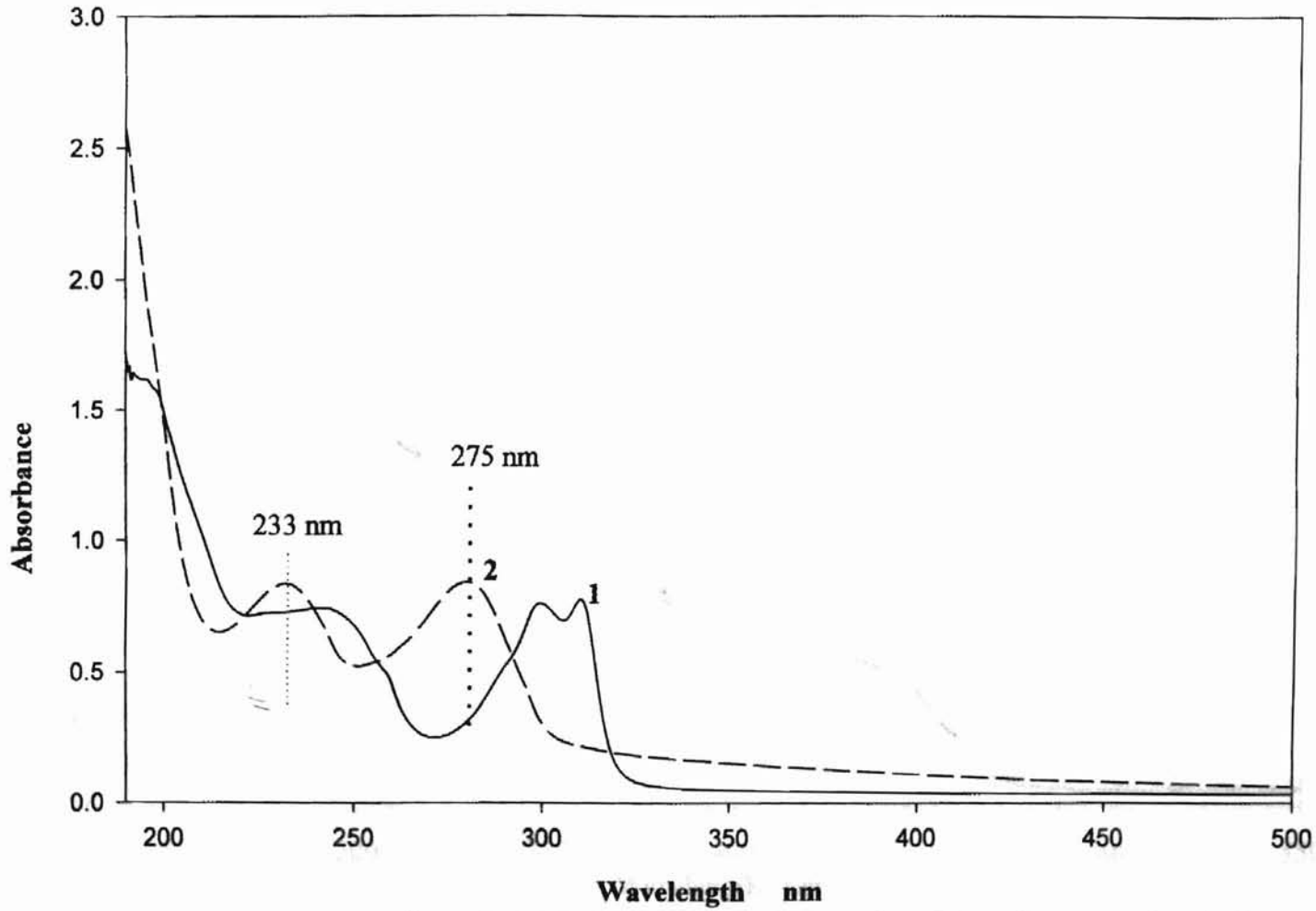

Fig. 21. UV absorption of CuBM/CdS-citrate and CuBM/Na_2S

1. CuBM; 2. CuBM with Na_2S

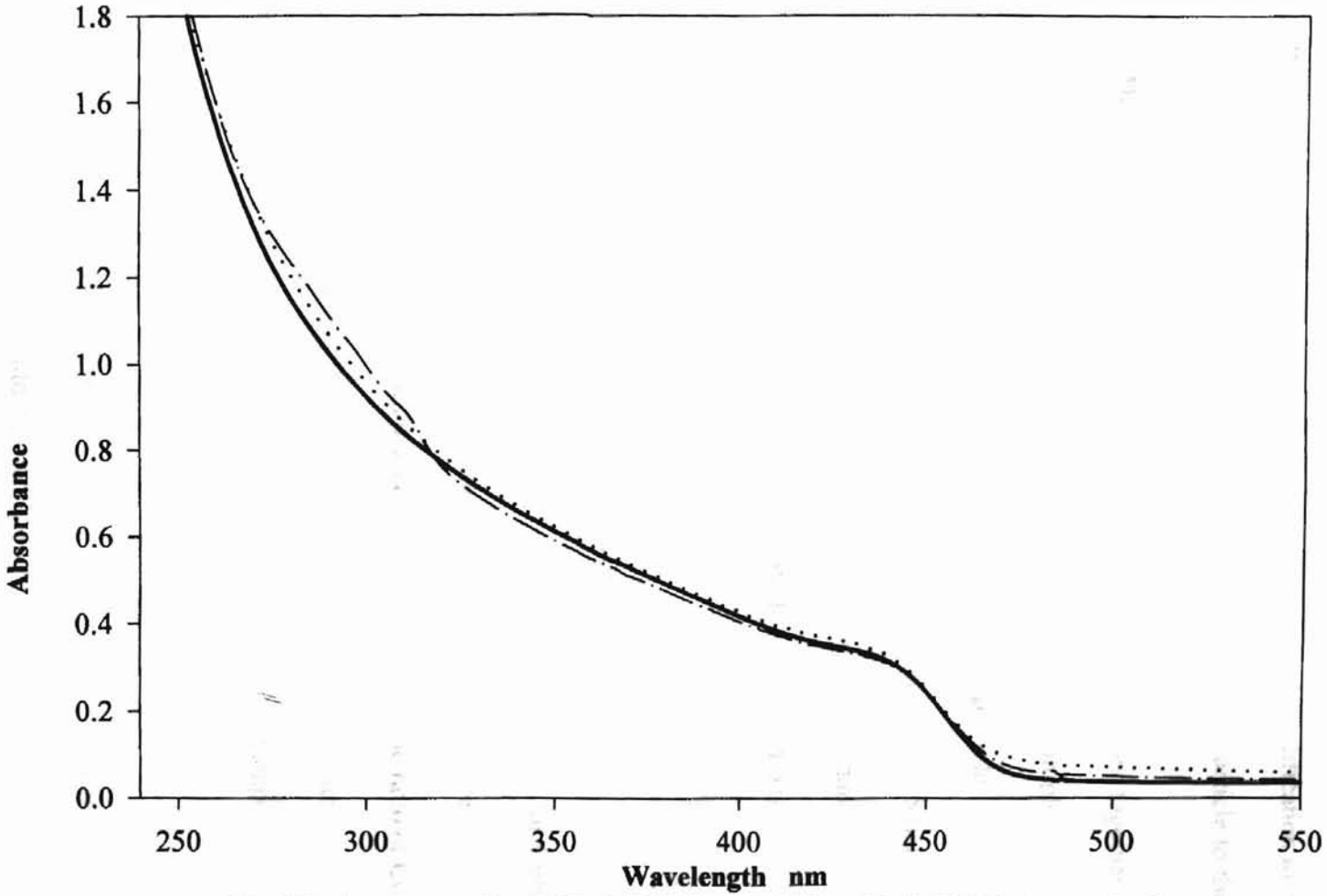

Fig. 22. UV absorption of modified CdS nanoparticle with CuBM before and after dialysis

— Unmodified CdS-citrate nanoparticles

–•– CdS-citrate modified by CuBM before dialysis, CdS-citrate/CuBM = 1:20

..... CdS-citrate modified by CuBM after dialysis, 48% of CuBM remained attached

Approximate calculation of the decrease in the CuBM absorption at 312 nm (CuBM absorption edge) shows that around 48% of CuBM still remained adsorbed (original CdS-citrate/CuBM = 1:20). The results of dialysis suggest that the modification to chalcogen sites is to some extend reversible, similarly to the derivation of nanoparticle to the metal sites.

b. TEM. TEM of CdS-citrate and modified CdS nanoparticles together with the size distributions obtained from TEM are given in Fig.23. CdS sample with an absorption maxima observed at 415 nm was chosen (same size nanoparticles were used for all the following experiment if not specified). Comparing the images of CdS nanoparticles before (a) & (c) and after (b) & (d) modification in Fig.23, the mean CdS nanoparticle sizes remain virtually the same being 3.28 nm and 3.31 nm, before and after modification respectively.

c. EPR. Experimental results accumulated for the reactions of copper II compounds with sulfide containing species[70] indicate that the copper ion of CuBM may undergo redox reaction upon binding to CdS surface. The oxidation state of Cu^{2+} for CuBM during the modification was monitored by EPR spectroscopy since Cu^{2+} is a $3d^9$ paramagnetic ion where Cu^{+} is $3d^{10}$ and is diamagnetic. At high concentration of CuBM-the ratio of CdS/CuBM was maintained 1:200, a weaker Cu^{2+} EPR signal is observed (Fig.24) after the modification. At low CuBM concentration, the EPR signal of Cu^{2+} is observed to disappear completely at high excess of CdS nanoparticles.

The decrease of the integrated signals of Cu^{2+} in Fig. 24 is calculated to be 63.9%. The decrease of the Cu^{2+} signal could be attributed to the reduction of Cu^{2+} to Cu^{+} and the reducibility of CdS-citrate is estimated to be around 120 CuBM molecules per particle. The

sites with stronger Lewis base activity (high negative charge) should react with CuBM with reduction of the central ion faster. In addition, they can also promote electron transfer from the surface of CdS to Cu^{2+}.

d. NMR . To obtain NMR spectrum and compare the signals of modified CdS with those of unattached free species, an appropriate amount of sodium citrate, malonic acid was directly dissolved in D_2O (99.9 atom % D) respectively. To dissolve bipyridine in D_2O, the solution was acidified by addition of HCl until initially opaque bipyridine in D_2O became clear. CdS-citrate was synthesized in D_2O (procedure the same as before), with the final concentration of Cd^{2+} estimated to be 1.6 mM and CdS-citrate:Cu^{2+} ratio to be1:40, no dialysis was applied.

The confirmation of the oxidation state change of copper could be obtained through ^1H NMR. $3d^9$ Cu^{2+} ions are paramagnetic and organic ligands attached to Cu^{2+} show no ^1H resonance signal due to the very fast T_2 relaxation time. As shown in Fig.25, the three weak but reproducible signals in the aromatic range could only be attributed to bipyridine ligand. The obvious broadening of the bipyridine signals suggests short relaxation time. This is indicative of the fact that the bipyridine remains bound to the copper center and through it to nanoparticles. The large mass frustrates tumbling which causes broadening. The signals show a little shift toward the upper field compared with the acidified free bipyridine, implies the increased electron density on the aromatic rings which could be pumped into the copper complex from the CdS conduction band.

In the upper field in Fig. 26, no sharp signal around 2.72 ppm originating from the free malonic acetate could be found.

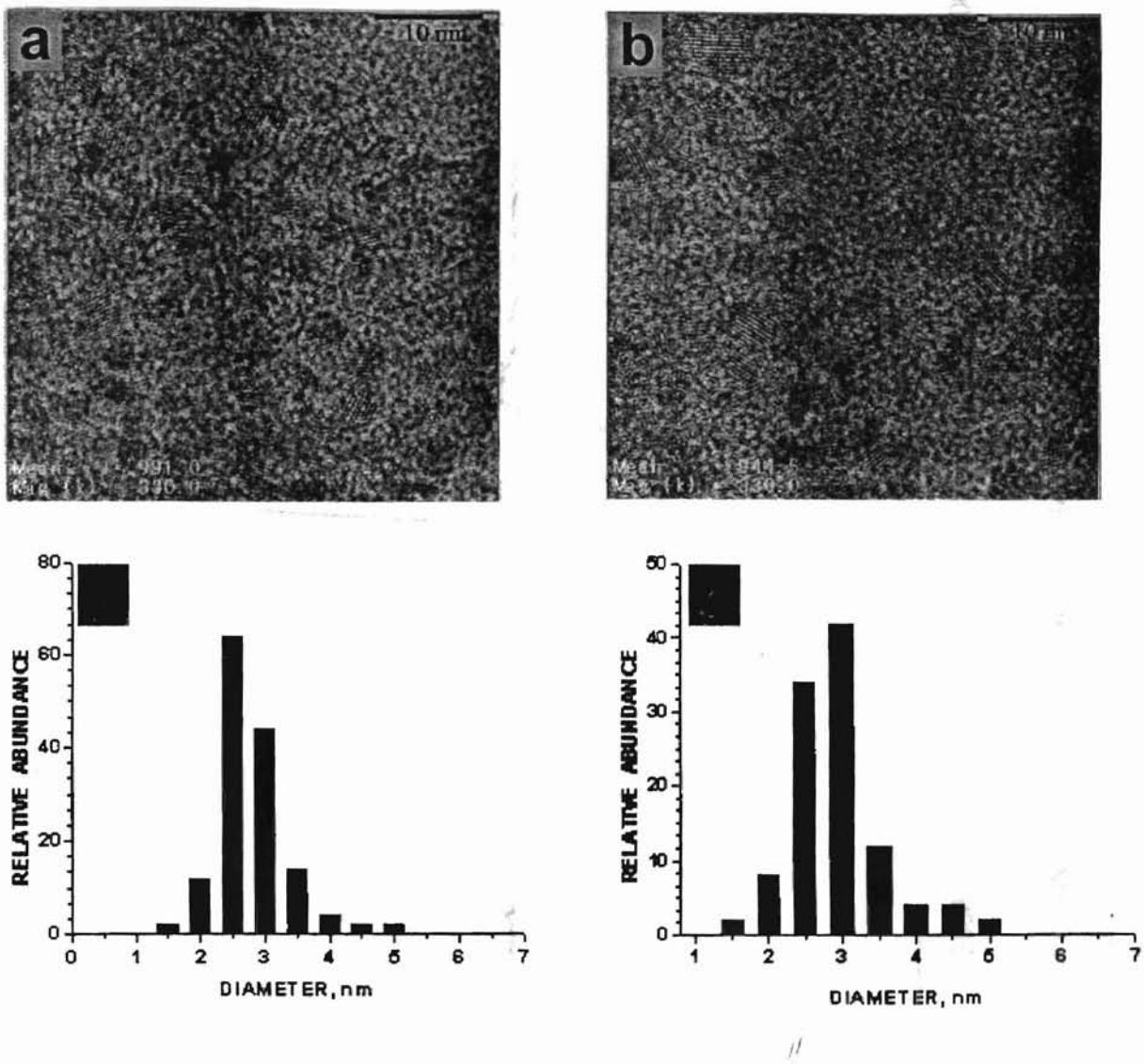

Fig. 23 TEM imagines of CdS-citrate nanoparticles before and after modification

a). CdS-citrate before modification

b). CdS-citrate after modification with CuBM

c). Size distribution of (a)

d). Size distribution of (b)

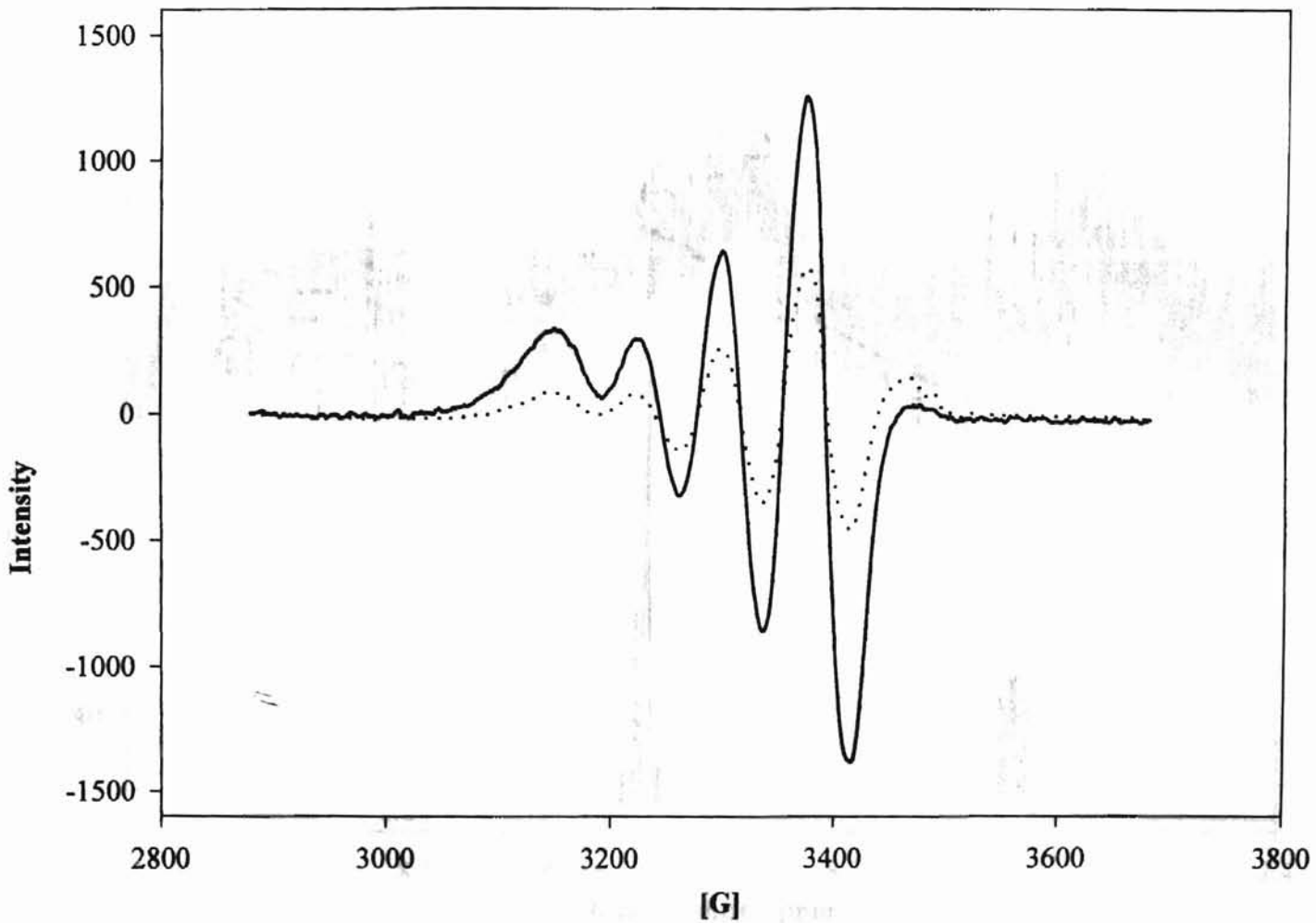

Fig. 24 EPR of CuBM before and after modification with CdS-citrate nanoparticles

—— CuBM in aqueous solution

..... CuBM after modification with CdS-citrate, CdS-citrate:CuBM = 1:200

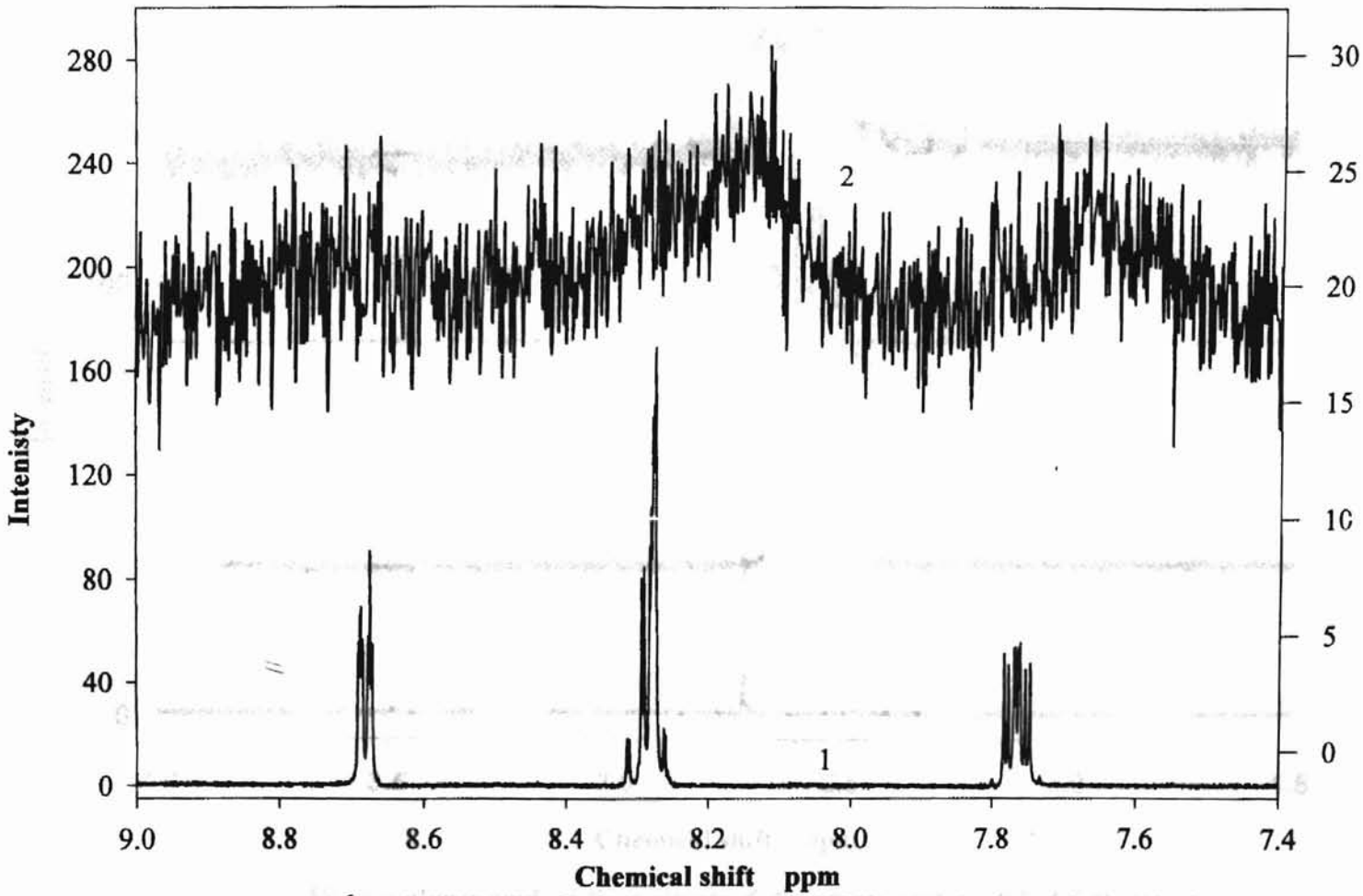

Fig. 25 ^{1}H NMR of Bipyridine and modified CdS-citrate with CuBM

1. Bypridine in acidified D_2O
2. Modified CdS-citrate with CuBM in D_2O

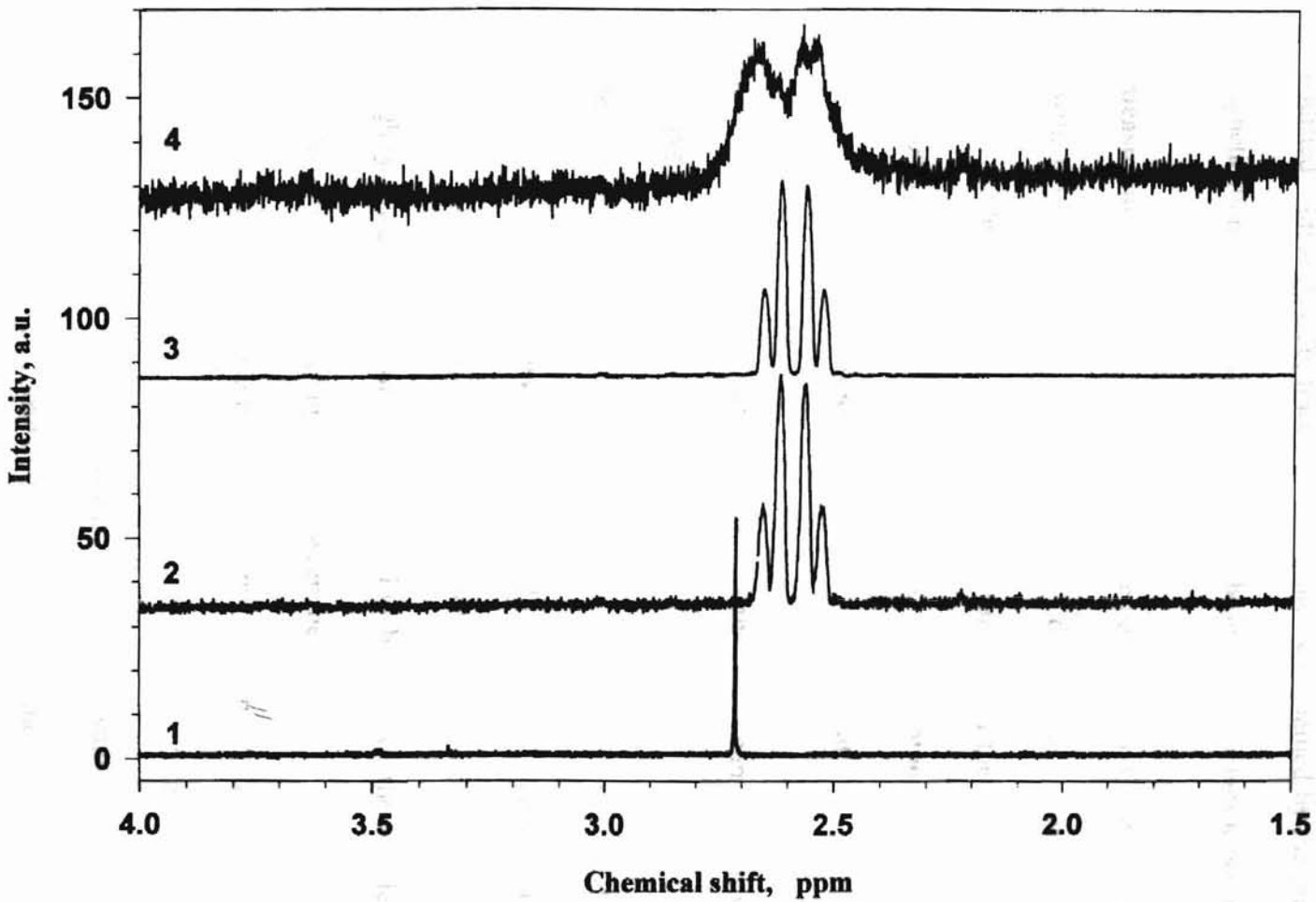

Fig. 26 ^{1}H NMR of malonic acid, sodium citrate, CdS-citrate and modified CdS-citrate
1. Malonice acid, 2. Sodium citrate, 3. Nonmodified CdS-citrate, 4. Modified CdS-citrate

It is concluded that the malonic acetate remains bound to the copper center after modification. Note that the citrate ion signals become very weak and significantly broadened in the modified sample (Fig.26, trace 4). This could be explained by the presence of Cu^{2+} whose magnetic moment causes the citrate ions in the immediate vicinity to become NMR-silent.

e. XPS measurement. Samples of a). CdS-citrate particles, b). CuBM, c). modified CdS particle with CuBM and d). dialyzed modified CdS particles were prepared for XPS measurements by leaving a drop of the aqueous samples on the clean surface of silicon wafers (cleaned by dipping the wafer into to 3% H_2O_2 in concentrated sulfuric acid solution, then rinsed thoroughly with DI water and ethanol) for vaporization.

Modification of the surface of CdS in reaction with CuBM can be clearly seen in XPS spectra. CuBM reveals typical Cu^{2+} peaks at 933.5 and 953.5 eV corresponding to Cu $2p_{1/2}$ and Cu $2p_{3/2}$ orbitals. They are also accompanied by a broad shake-up band located at 944 eV. After the reaction with CdS nanoparticles, the $2p_{1/2}$ and $2p_{3/2}$ signals become broader and shift to 932.5 and 952.5 eV (Fig. 27, A). These binding energies are typical for Cu^{+}, which require slightly lower energy for electron ejection because of the smaller charge. The decrease of intensity for the shake-up band between the two major signals also indicates the reduction of Cu^{2+} to Cu^{+} because this band can not be seen for the one- and zero- valent copper. Notably, the shape of Cu $2p_{1/2}$ and Cu $2p_{3/2}$ bands after the modification is complex revealing the presence of several components. This demonstrates the presence of Cu in several oxidation states, which corroborates with the EPR findings.

Effect of the modification on surface sulfur atoms can be seen in 160-170 eV region (Fig. 27, B).

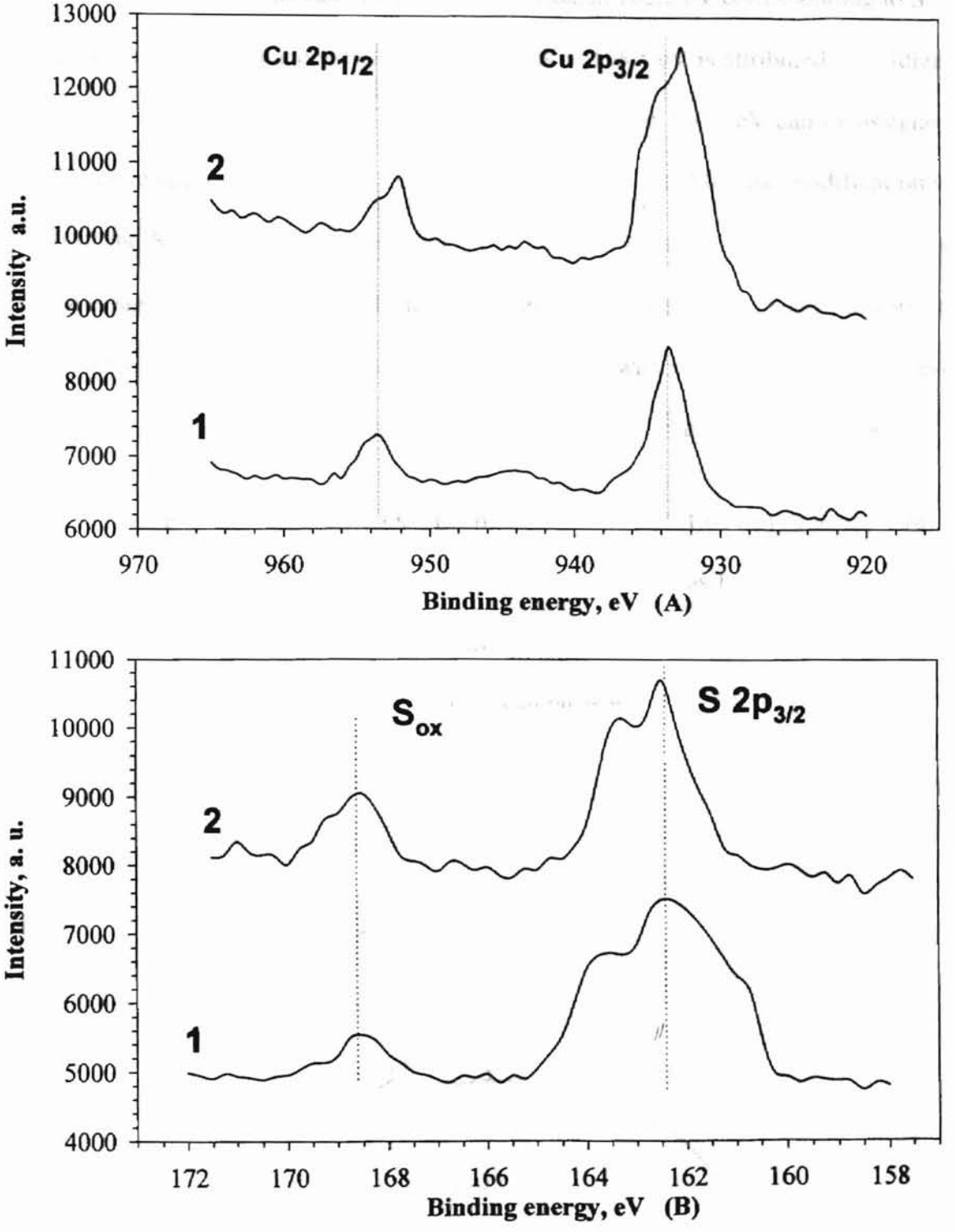

Fig. 27 XPS signals of Cu and S before and after modification

1. Before modification
2. After modification

For CdS nanoparticles one can observe a broad signal at 162.5 eV corresponding to S $2p_{3/2}$ orbitals located in the nanoparticle core. The peak at 168.5 eV is attributed to oxidized S atoms located on the surface of CdS, while the shoulder at 160.6 eV can be assigned to negatively charged sulfur species on the nanoparticle surface. After the modification with CuBM, the XPS spectrum of the sulfur atoms changes significantly: the 162.5 eV peak becomes significantly narrower and the shoulder at 160.6 eV disappears. Such transformation is consistent with the reaction of the surface sulfur atoms with metal complex, which results in disappearance of the surface states of sulfur responsible for the shoulder at 160.6 eV.

Based on the above information obtained through various spectroscopy, a model structure of the CuBM-modified CdS nanoparticles can be represented as Fig. 28. As compared to scheme 3 on page 40, the result of the modification is not limited to the replacement of H_2O ligand. The partial reduction of Cu^{2+} to Cu^{+} also takes place, which is proven by UV-vis, EPR and XPS data.

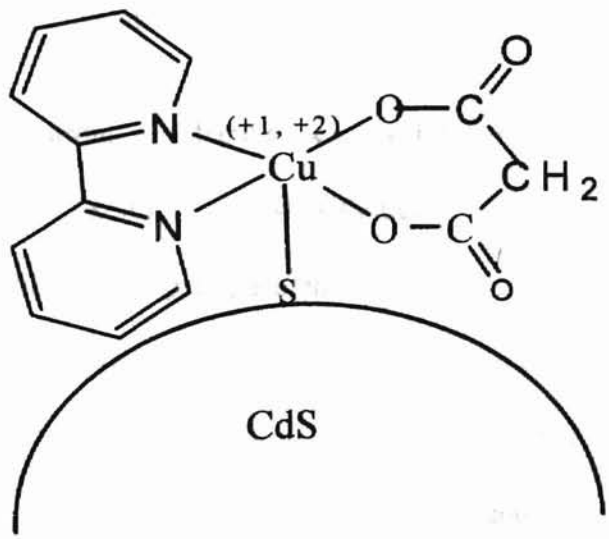

Fig. 28 Structure of modified CdS-citrate nanoparticle with CuBM

2. Optical properties of CuBM-modified CdS-citrate nanoparticles

The effect of modification on the optical absorption of CdS nanoparticle is shown in Fig. 18 and 19. The red shift and broadening of the absorption edge of nanoparticles reveal the perturbation of energy levels of the CdS core. More sensitive measurements are carried out by fluorescence spectroscopy.

a. Photoluminescence. Study of the influence of modification with CuBM on the emission of CdS nanoparticle is given in Fig.29. CdS-citrate nanoparticles of different size were chosen with distinguishable excitonic peak around 423, 432, 445 nm respectively and the particle diameter of 26, 30, 35 Å. The trapped emission maxima of broad multicomponent bands for the non-modified CdS particles are located at 618, 628 and 670 nm. For all three size particles, after modification with CuBM, the trapped emission bands originated from the surface states become weaker and shift further to the red. This fact suggests the reconstruction of the particle surface, which is expected for the modification reaction involving the formation of covalent bonds to the surface atoms of nanoparticles.

In the band gap region, a strong new band appears with the maxima around 447 nm, which overlaps with the weaker excitonic bands. Although it is located in the vicinity of the excitonic emission, it shows no dependence on the particle size and therefore, corresponds to a transition other than the first exciton. The incorporation of copper ions into II-VI and other semiconductors is known to result in the radiative transition between the conduction band and the copper centers[71]. Therefore, the new band around 447 nm can be attributed to the transition between the conduction band of CdS and the atomic d-energy level of copper from the Cu-bipyridine units bound to the CdS surface (Fig.30).

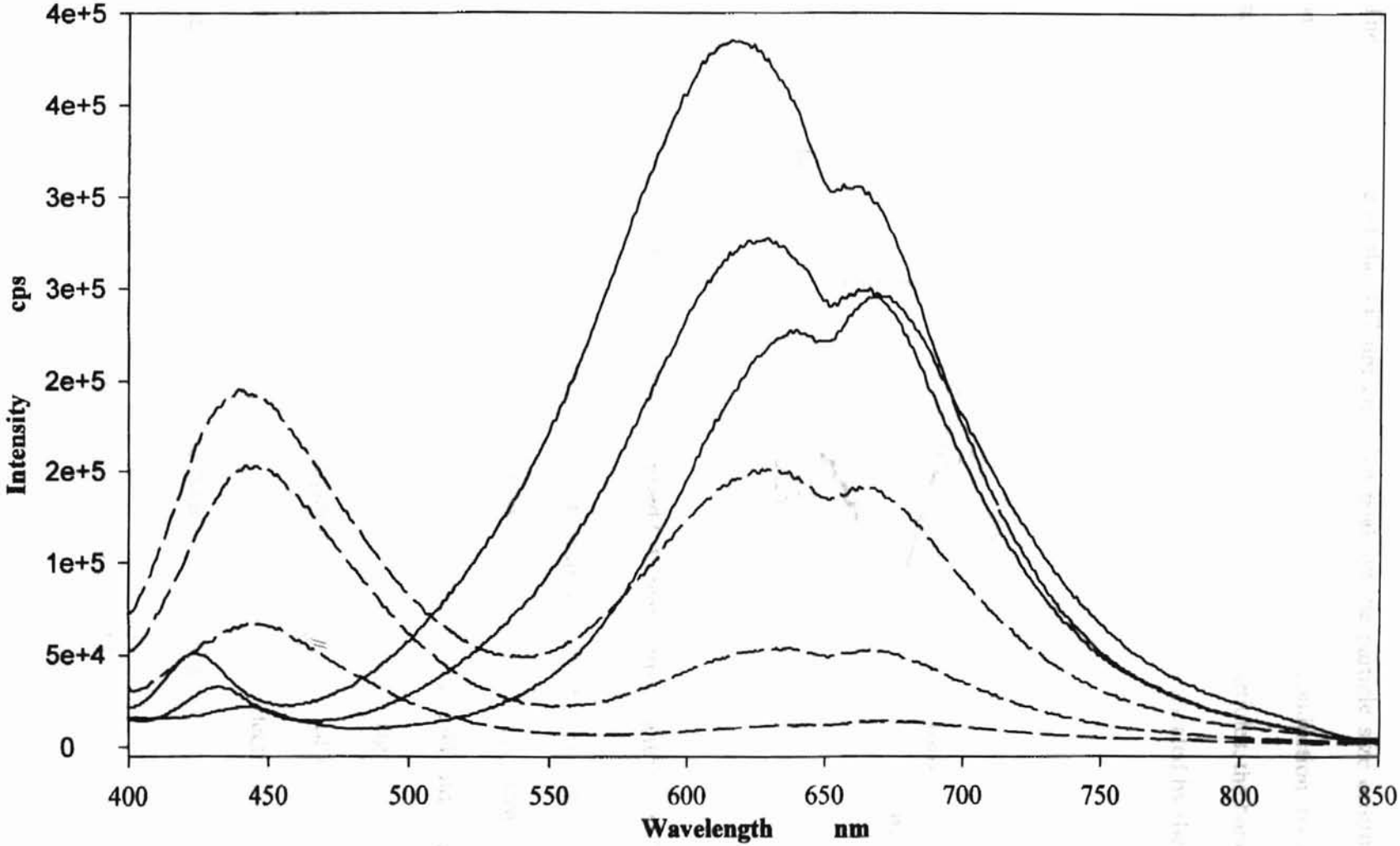

Fig. 29 Modification of different size CdS-citrate nanoparticle with CuBM (CdS-citrate:CuBM=1:60)
___ Unmodified CdS-citrate nanoparticles
- - - Modified CdS-citrate nanoparticle with CuBM

The independence of the 447 nm emission peak on the particle size originates from a virtually constant position of the absolute energy of the conduction band for II-VI nanoparticles as the particle size changes. For fairly large nanoparticles, the band gap varies primarily due to the shift of the energy of the valence band as indicated by theoretical and experimental data[72].

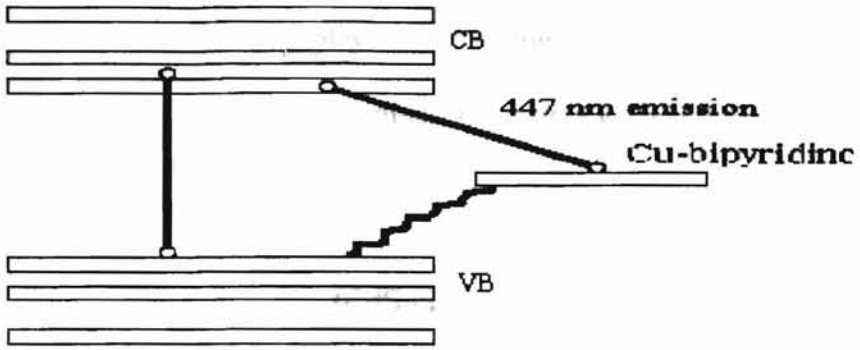

Fig. 30. Energy diagram of modified CdS nanoparticle with CuBM

However, the 447 nm emission peak could originate from other sources such as: 1).Strongly altered emission due to hybridization emission from the d-d transition in Cu^{+}. 2). Luminescence from the by-product of the modification reaction. The 447 nm emission peak was treated, based on the current data, as an intrinsic spectroscopic signature of the CuBM modification of CdS. Spectroscopic investigation of the genesis of 447 nm peak is of tremendous fundamental importance for understanding the electronic processes in nanoparticles and will be the subject of the future investigation,

The modification of CdS with different CdS-citrate/CuBM ratio of is shown in Fig.31 together with the emission of CdS-citrate nanoparticle in the presence of $CuCl_2$. An increasing trend of the 447 nm emission band and a quenching of the trapped emission band

can be noticed as the ratio of CdS/CuBM increases from 1:0 to 1:30 , 1:60 and 1:90. As the ratio reaches 1:90, the trapped emission bands almost disappear completely, indicates that the surface states are all quenched by CuBM. For $CuCl_2$, a quenching effect for the trapped emission and a small increase in the excitonic emission region can be observed, which can be attributed to partial replacement of surface Cd^{2+} with Cu^{2+} ions[70]. Importantly, there is no rise around 447 nm for the CdS-citrate-$CuCl_2$ system, which implies that the heterocyclic ligand of bipyridine on the CuBM plays a determining role in the modification and is responsible for the formation of surface luminescing energy level between CdS particles and CuBM.

Dialysis of modified CdS with CuBM (CdS-citrate:CuBM = 1:90) was carried out and the emission measurements taken. The trapped emission could recover from 3% to 62.7% after dialysis while a less intense peak remained around 447 nm (Fig.32). The decrease of 447 nm peak is calculated to be 61.7%, suggesting the reversible adsorption and desorption of CuBM onto the nanoparticle surface. Some amount of Cu-bipyridine still remained bound to the surface sulfide ions, which is in consistent with UV absorption data.

b. UV Light induced modification study. During the emission measurement, a remarkable growth of 447 nm peak could be noticed. The intensity growth was noticed to be much faster during the emission scan (4 s per nm scan rate) than storing the solution in dark several hours for the modification to complete, which led us to believe that the modification is light-induced.

To obtain the information as which wavelength region could most efficiently induce the modification, a batch of CdS/CuBM (CdS-citrate:CuBM = 1:60) samples were irradiated for

80 minutes each separately with a monochromatic light starting from 270 nm to 460 nm, with a wavelength interval of 5 nm, bandpass 2 nm. The emission intensity at 447 nm was plotted versus the irradiating light wavelength (Fig.33). The profile of this plot resembles the sum of the UV absorption for CuBM and CdS, indicating that excitation of both CuBM and CdS results in band formation between CdS and CuBM .

The light-induced modification process was also monitored by the fluorescence spectroscopy as shown in Fig.34. Modified CdS-citrate sample was irradiated with a monochromatic light of 305 nm (most efficient light region) with a bandpass of 5 nm. Monitoring of the luminescence intensity versus the time of irradiation reveals that the maximum intensity of 447 nm peak can be reached within 160 minutes. Smaller change can be observed for the trapped emission band. The corresponding UV absorption spectra (Fig. 35) of the modification kinetics reveals that the relative intensity of the 277 nm absorption shoulder increases considerably during the irradiation. A significant decrease in the absorption maxima of CdS bands as well as CuBM band and an absorption increase in the CdS UV-vis tail can be seen. Similarly to Fig. 18, an isobestic point forms in the interval of wavelengths corresponding to the CdS absorption onset.

The appearance of the 277 nm band is indicative of the formation of Cu-S bonds during the irradiation (see Fig. 20, 21). It is conceivable that photoexcitation of both the nanoparticle and CuBM stimulates binding of the complex to nanoparticle surface.

Dialysis for 12 hours against 18 MΩ water was carried out for the modified CdS-citrate nanoparticles after the irradiation for 160 minutes. UV absorption for the dialyzed sample is also presented in Fig. 35.

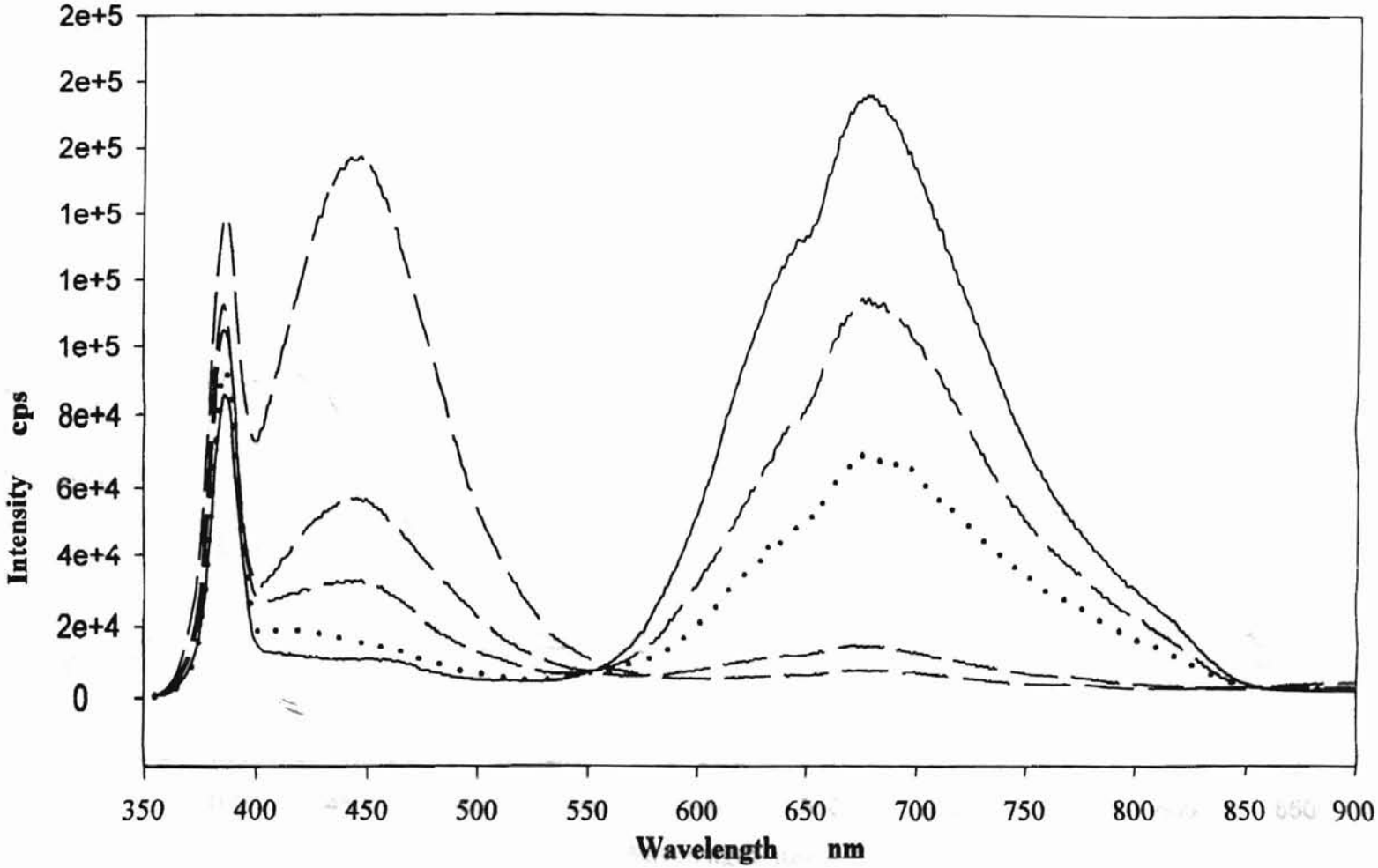

Fig. 31 Emission of modified CdS-citate nanoparticle at different CuBM concentration and with $CuCl_2$

Excited at 340 nm, filter cut off at 395 nm

___ Unmodified CdS-citrate nanoparticle

---- Modified CdS-citrate at CdS-citrate:CuBM equals to 1:30, 1:60, 1:90

..... Modified CdS-citrate with $CuCl_2$ at CdS-citrate:$CuCl_2$ equals 1:60

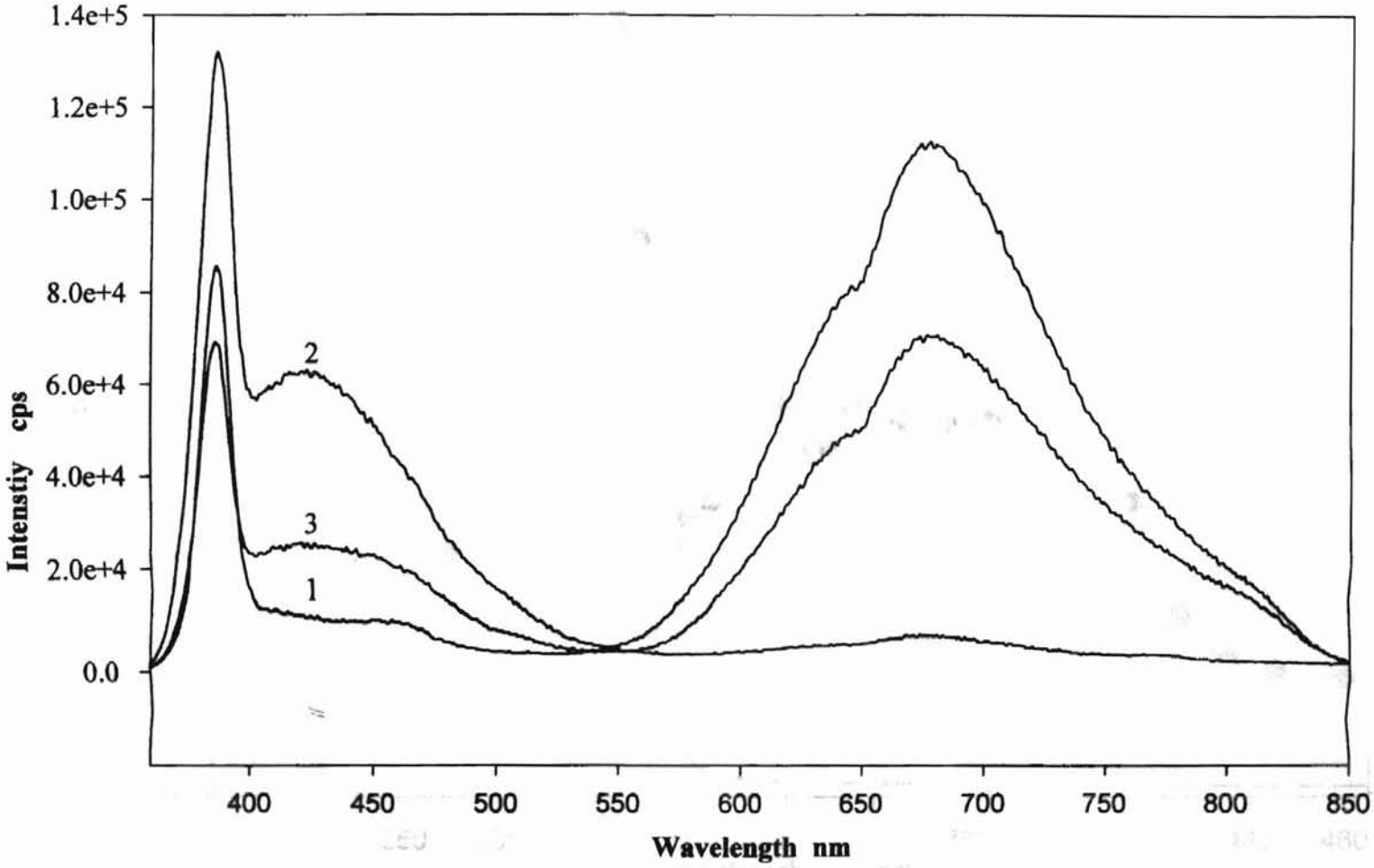

Fig. 32. Emission of modified CdS-citrate nanoparticles before and after dialysis
Excited at 340 nm, filter cut off at 385 nm

1. Non modified CdS-citrate nanoparticles
2. Modified CdS-citrate nanoparticle before dialysis
3. Modified CdS-citrate nanoparticle after dialysis against water

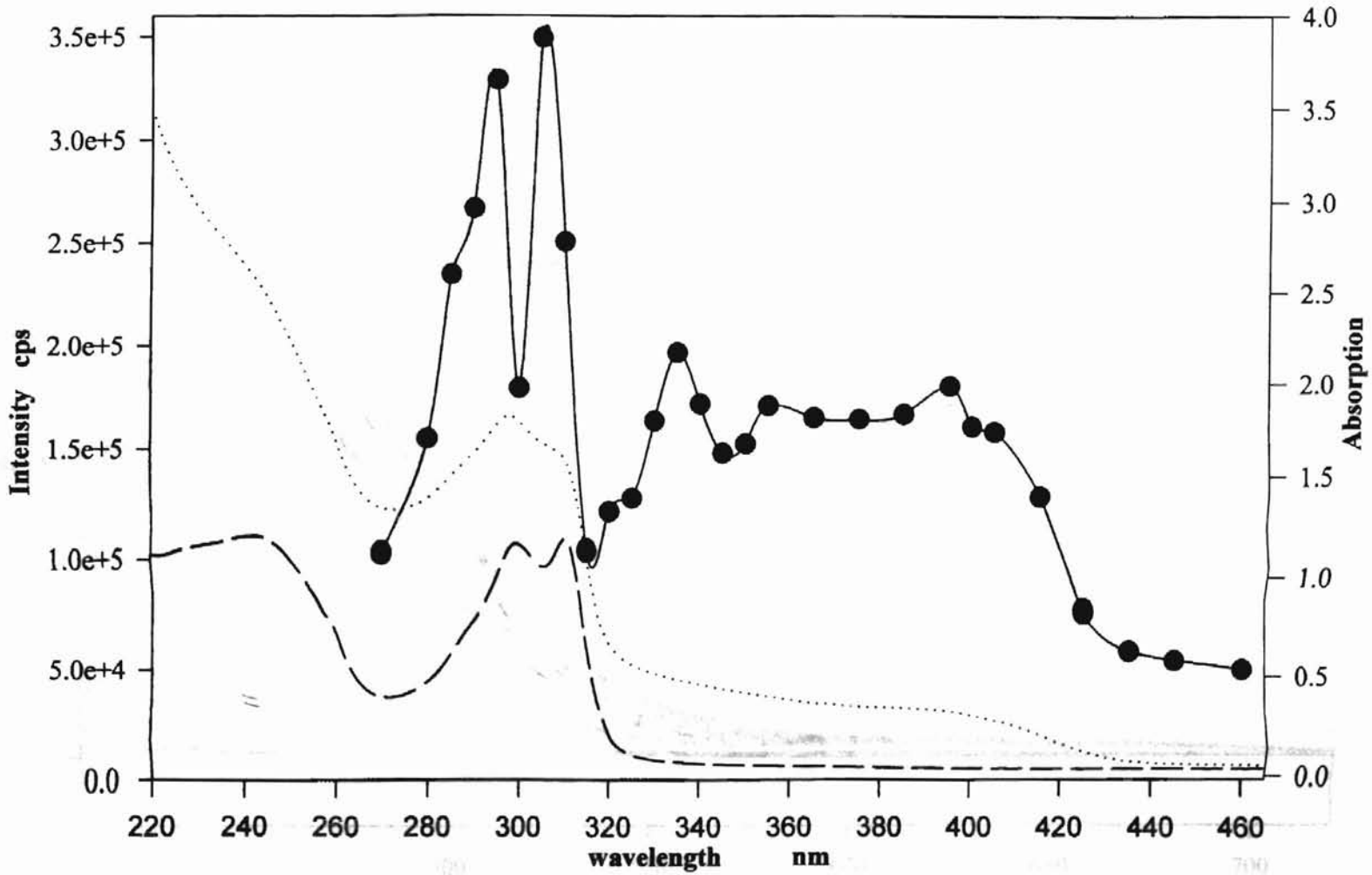

Fig. 33 Light induced modification at different irradiation wavelength monitored as 447 nm peak intensity

..... UV obsorption of modified CdS-citrate nanoparticle with CuBM

---- UV absorption of CuBM

___ 447 emission peak intensity at different irradiating light wavelength

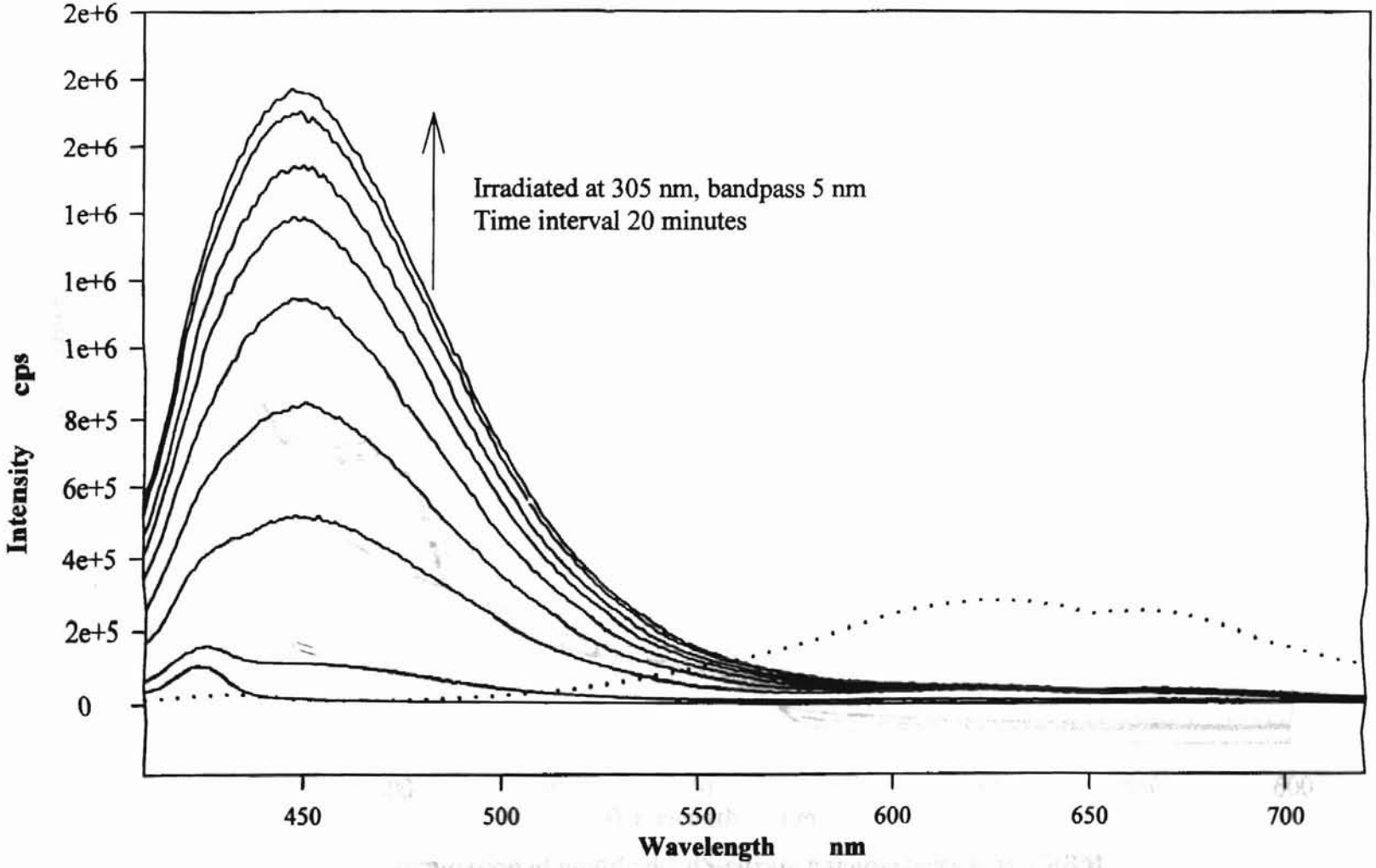

Fig. 34 Modification of CdS-citrate nanoparticles with CuBM by irradiation

Excited at 370 nm, filter cut off at 385 nm

.....Unmodified CdS-citrate nanoparticles

——Modified CdS-citrate nanoparticle during irradiation, time interval 20 minutes

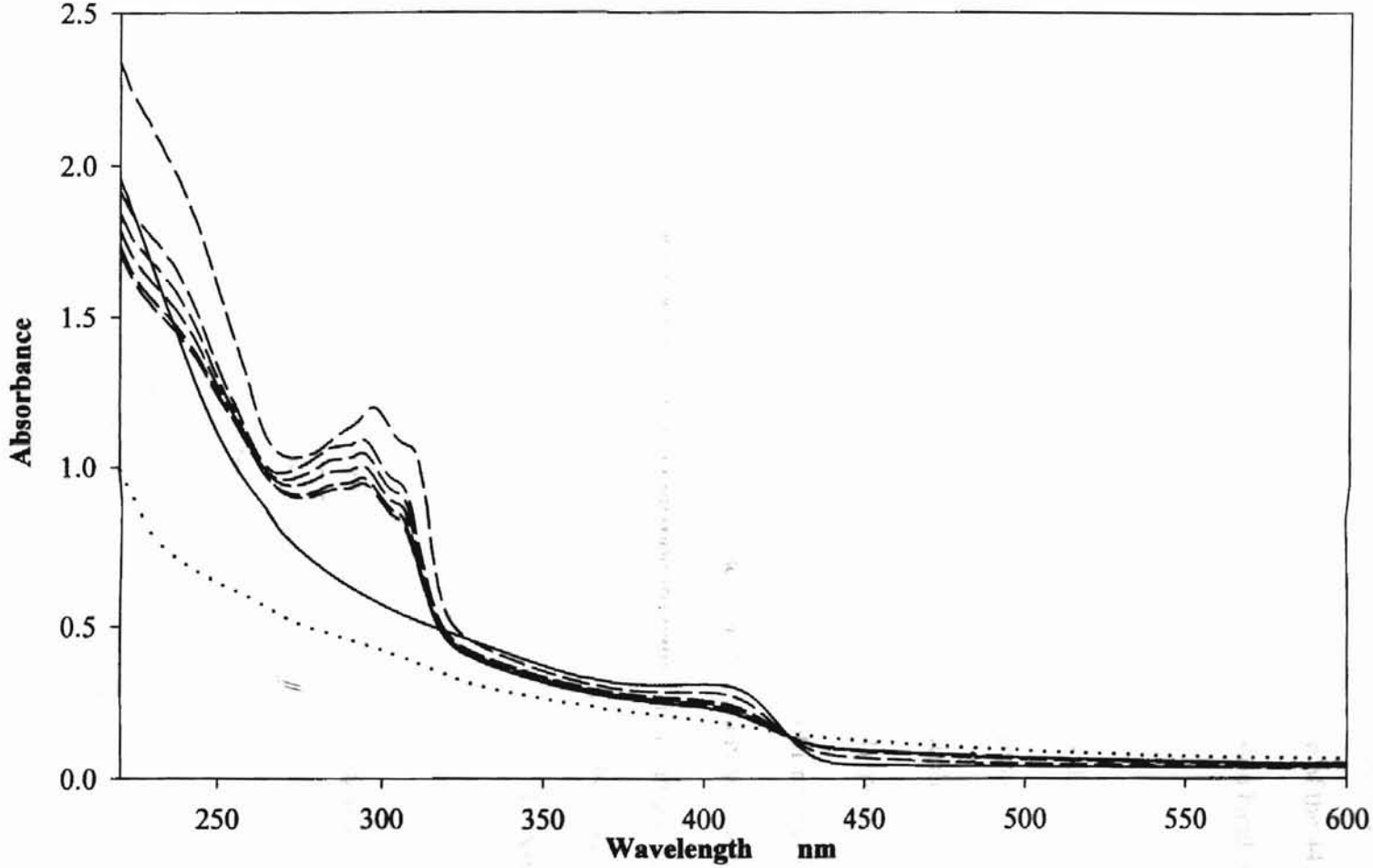

Fig. 35. Irradiation of modified CdS-citrate nanoparticles with CuBM

— Non-modified CdS-citrate nanoparticle

- - - Irradiation of modified CdS sample monitored every 20 minutes

..... Irradiated CdS-citrate/CuBM after dialysis against water

Two weak shoulders could be observed in the CuBM absorption region, indicating that some amount of CuBM remain attached to CdS particle surface after the dialysis. The emission spectrum for the dialyzed sample is shown in Fig. 36. The decrease of the 447 nm peak after dialysis is calculated to be 66.1%. No recovery of the trapped emission band is observed after dialysis.

The quantum yield of samples of CdS nanoparticle stabilized by sodium citrate (sample 1), CdS-citrate modified by CuBM without UV light irradiation (sample 2), modified CdS by irradiation (sample 3) were calculated by comparing the individually integrated emission peaks with the integrated peak area around 560 nm of a freshly prepared rhodamine B ethanol solution, using the excitation wavelength at which both rhodamine B and CdS showed the same optical density (345 nm was used for this study with a filter of 395 nm wavelength cut off placed before emission monochromator). For sample 3, the irradiation lasted for 160 minutes for the 447 nm peak to reach maxima. All CdS emission peaks were Gaussian fitted with 4 parameters using SigmaPlot and integrated by GRAMS/386. Baseline integration was used. The quantum yield changes are given in Table 3.

Table 3. Quantum Yield of Excitonic, Trapped Emission and 447 nm Peak

	Sample 1	Sample 2	Sample 3
QY[1] of 414 nm	0.251%	0.104%	--
QY[2] of 447 nm	--	--	4.790%
QY[3] of 650 nm	7.473%	2.411%	6.021%

1. Quantum yield of the excitonic peak at 414 nm.
2. Quantum yield of 447 nm peak
3. Quantum yield of the trapped emission from 550 nm to 750 nm

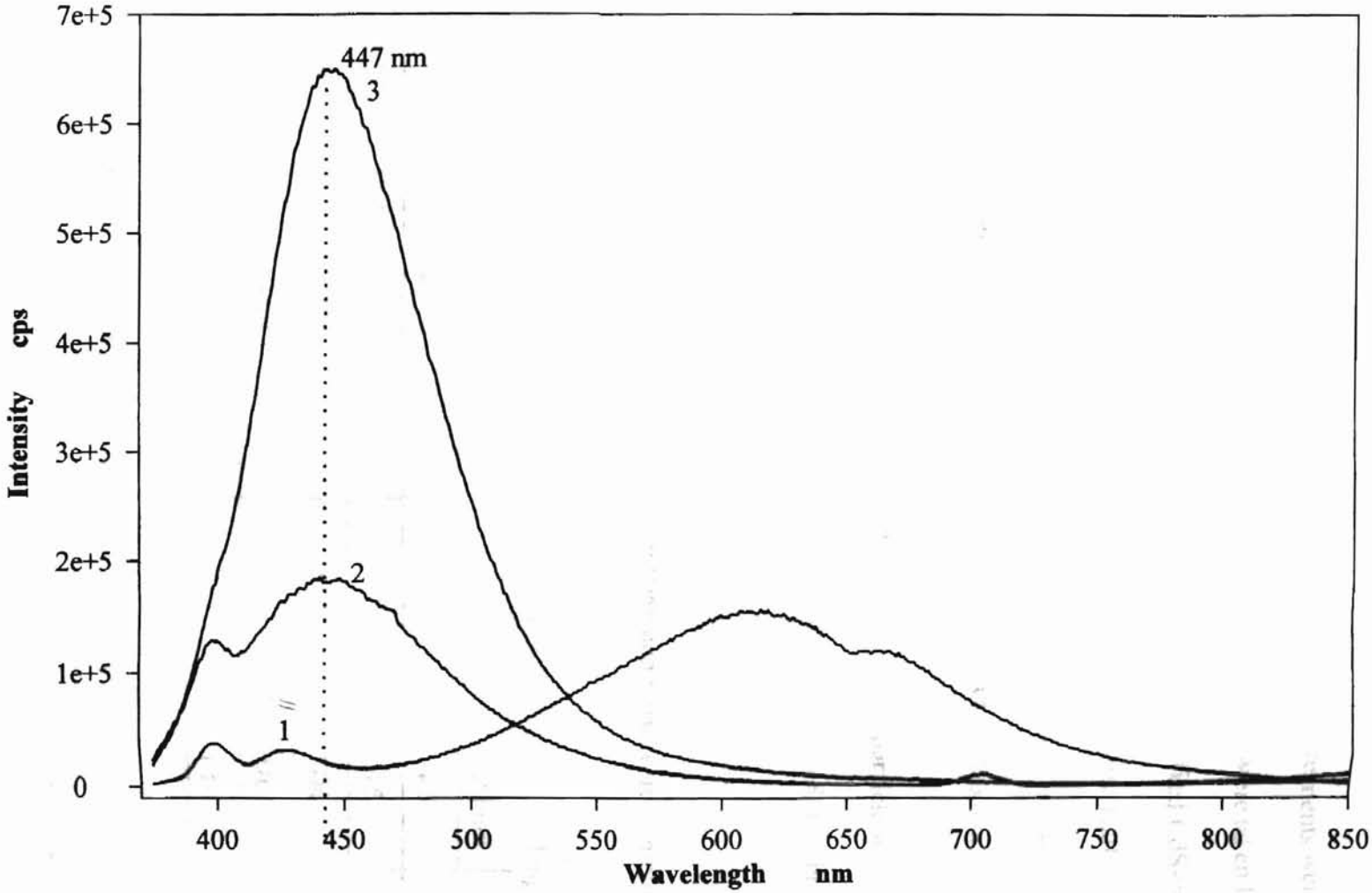

Fig. 36 Emission of the irradiated CdS-citrate/CuBM supramolecule before and after dialysis

1. Non-modified CdS-citrate nanoparticles
2. Irradiated CdS-citrate/CuBM supermolecule for 160 minutes before dialysis
3. dialyzed sample of trace 2. (Intensity decreased by 66.1%)

c. Time-resolved photoluminescence. Samples for TRPL measurements were prepared the same as for the light induced modification studies. Measurements were taken for the samples of nonmodified CdS-citrate nanoparticles (Cd^{2+}:S^{2-} = 4:1), modified CdS-citrate particles with CuBM, with the estimated CdS-citrate:CuBM ratio equals 1:20 (CdSCu1), 1:40 (CdSCu2), 1:60 (CdSCu3), 1:80 (CdSCu4) after irradiation with a monochromatic light of 305 nm with various time periods for the 447 nm peak to reach maxima.

The life-time for the excitonic peak of nonmodified CdS-citrate particle was measured to be 18.7 ns, while the life-time for the trapped emission band is 65~78 ns. The other data are listed in table 4.

Table 4. Life Time of Exciton, 447 nm Peak and Surface Recombination

Samples/Life time (ns)	Life time (ns) at peak maxima wavelength of:			
	414 nm	447 nm	580/620 nm	651/660 nm
Nonmodified CdS-citrate	18.7	-	64.3	78.0
CdSCu1 (CdS/Cu=1/20)	-	5.3	115	131
CdSCu2 (CdS/Cu=1/40)	-	5.4	104	128
CdSCu3 (CdS/Cu=1/60)	-	4.8	96	102
CdSCu4 (CdS/Cu=1/80)	-	4.6	110	115

The life-time of 447 nm peak remains practically unchanged within the experimental error of the technique. After the modification, the life-time of the surface recombination increases significantly from 64~78 ns to 110~130 ns. Hardly noticed, dependence of the life-time in CuBM-modified CdS suggests quite fast transition from CB of CdS to the d-level of copper

(see Fig. 3), which makes the efficiency of population of the intra band gap level quite insensitive to the total number of CuBM units attached. This correlates well with the life-times obtained for the 447 nm band (Table 4). If one compares the luminescence kinetics of the 580/620 and 651/660 bands in modified and non-modified CdS, the life-times in CdS/CuBM are substantially longer. While stating this fundamentally important fact, we need to note that numerous relaxation processes should be considered to understand its origin. One of the possibilities is the life-time elongation due to the delocalization of surface electrons or holes in the aromatic rings of the modifier. Development of the spectroscopic techniques to establish the nature of the electronic transitions in CuBM-modified CdS can be one of the extensions of this study.

C. CONCLUSIONS.

Citrate-ion-stabilized, size controlled CdS, CdSe nanoparticles were synthesized. The prepared nanoparticles were characterized by TEM, optical absorption, photoluminescence and XRD.

Citrate-ion-stabilized CdS nanoparticles were used in chalcogenide site modification by CuBM. The structure of modified nanoparticles was proposed based on the information obtained through UV-vis absorption, TEM, EPR, NMR and XPS spectroscopy. It was established that the modification results in replacement of aqua ligand in CuBM, formation of Cu-S bond with surface S-atoms of CdS and partial reduction of Cu(II) to Cu(I).

The optical properties of modified CdS particles were studied. The spectroscopic signature of the surface modification was found to be the strong luminescence peak at 447 nm, which

does not depend on the CdS particle size.

Surface modification of CdS can be facilitated by light illumination. The excited states of both CdS and CuBM are involved in the photoinduced reaction.

Reference List

1. Levy, R.J., Labhasetwar, V., Underwood, T., Song, C., Chen, W. Bioact. Mater. Vol. 24, 1997, 189-190.

2. Maruyama Atsushi, Ishihara Tsutomu, Kim Jin-Seik, Kim Sung Wan, Akaike Toshihiro, Colloids Surf., A Vol. 153(1-3), 1999, 439-443

3. Murphy Catherine J., Brauns Eric B., Gearheart Latha, MRS Symp. Pro. Vol. 452, 1996, 597-598

4. Labhasetuar V., Song CX., Levy RJ., Advanced Drug-Delivery Reviews Vol. 24, 1997, 63-85

5.Viswanadham, G., Elghanian, R., Mirkin, C. A., Letsinger, R. L. Book of Abstracts, 218th ACS National Meeting, New Orleans, Aug. 22-26, 1999.

6. Li M.Q., Xu H.X., Z J., Ji A., He B.L., Pang Y., Huang J.Y., Niu R.F., Sci. China Ser. B: Chem Vol. 39(6), 1996, 577-584

7. Kresse, M., Pfefferer, D., Thode, K., Mueller, R. H., Semmler, W., World Meet. Pharm., Biopharm. Pharm. Technol., Vol. 1, 1995, 507-508

8. Chechik, Victor; Zhao, Mingqi; Crooks, Richard M., Book of Abstracts, 218th ACS National Meeting, New Orleans, Aug. 22-26, 1999

9. Bard A.J., Science Vol. 207, 1980, 4427

10. Bard A.J., Ber. Bunsen-Ges. Phys. Chem. Vol. 92, 1988, 1194-1198

11. Bera P, Patil K.C., Jayaram V., Hegde M.S., Subbanna G.N., J. Mater. Chem. Vol. 9(8), 1999, 1801-1806

12. Boronina T.N., Dieken L., Lagadic I., Klabunde K.J., J. Hazard. Subst. Res. 1998, 1 No pp given

13. Moscovici J., Michalowicz A., Decker S., Lagadic I., Latreche K., Klabunde K., J. Synchrotron Radiat. Vol. 6(3), 1999, 604-606

14. Tanaka K., Recent Progress in Microcrystalline Semiconductor Thin Films; MRS Symp. Pro. Vol. 452, 1996, 3-17

15. Motte L., Petit C., Boulanger L., Lixon P., Pileni MP., Langmuir Vol. 8, 1992, 1049-1053

16. Petit C., Pileni MP., J. Phys. Chem. Vol. 92, 1988, 2282-2286

17. Petit C., Lixon P., Pileni MP., J. Phys. Chem. Vol. 94, 1990, 1598-1603

18. Lianos P., Thomas J.K., Chem. Phys. Lett. Vol. 125, 1986, 299-302

19. Meyer M., Wwallberg C., Kurihara K., Femdler J.H., J. Chem. Soc., Chem. Commun. 1984, 90-91

20. Steigerwald M.L., Alivisatos A.P., Gibson J.M., Harris T.D., Kortan R., Muller A.J., Thayer A.M., Duncan T.M., Douglass D.C., Brus L.E., J. Am. Chem. Soc. Vol. 110, 1988, 3046-3050

21. Spanhel L., Haase M., Weller H., Henglein A., J. Am. Chem. Soc. Vol. 109, 1987, 5649-5655

22. Fendler J.H., Chem. Rev. Vol. 87, 1987, 877-898

23. Seal S., Bracho L., Shukla S., Morgiel J., J. Vac. Sci. Technol., A Vol. 17(5), 1999, 2950-2956

24. Wang Y.Q., Cheng H.M., Hao Y.Z., ma J.M., Li W.H., Cai S.M., Thin Solid Films Vol. 349(1, 2), 1999, 120-125

25. Parvathy N.N., Pajonk G.M., Rao A.V., India. Nanostruct. Mater. Vol. 8(7), 1998, 929-943

26. Gutierrez M., Henglein A., Ultrasonics Vol. 27, 1989, 359-362

27. Thurner J.E., Henderwerk M., Parmeter J., Somorjai G.A., J. Electrochem. Soc. Vol. 131, 1984, 1777

28. Xu J.F., Ji, W., J. Mater. Sci. Lett. Vol. 18(2), 1999, 115-117

29. Murray C.B., Norris D.J., Bawendi M.G., J. Am. Chem. Soc., Vol. 115, 1993, 8706-8715

30. Yoshihisa Ohko, Masanobu Setani, Takao Sakata, Hirotaro Mori, Hiroshi Yoneyama, Chem. Lett., 1999, 663-664

31. Fischer C.H., Weller H., Katsikas L., Henglein A., Langmuir Vol. 5, 1989, 429-432

32. Eychmueller A., Katsikas L., Weller H., Langmuir Vol. 6, 1990, 1605-1608

33. Sivamohan R., Kasuya A., J. Elec. Mater., Vol. 28(5), 1999, 442-444

34. Wei G.T., Liu F.K., Wang C., Analy. Chem., Vol. 71(13), 1999, 2087-2091

35. Fischer C.H., Siebrands T., J. Chromatog. A, Vol. 707, 1995, 189-197

36. Nanda K.K., Sarangi S.N., Sahu S.N., Deb S.K., Behera S.N., Physica B Vol. 262(1&2), 1999, 31-39

37. Henglein A., Chem. Rev. Vol. 89, 1989, 1861-1873

38. Rogach, A. L., Kornowski, A., Gao, M.Y., Eychmueller, A., Weller, H., J. Phys. Chem. B Vol. 103(16), 1999, 3065-3069

39. Chestnoy N., Harris T.D., Hull R., Brus L.E., J. Phys. Chem. Vol. 90, 1986, 3393-3399

40. Chen W., Wang, Z.G., Lin, Z.J., Lin, L.Y., J. Appl. phys. Vol. 82(6), 1997, 3111-3115

41. Scolan E., Scanchez C., MRS Symp. Pro. Vol. 519, 1998, 329-335

42. Ladizhansky V., Hodes G., Vega S., J. Phys. Chem. B Vol. 102, 1998, 8505-8509

43. Vossmeyer T., Reck G., Katsikas L., Haupt E.T.K., Xchulz B., Weller H., Science Vol. 267, 1995, 1476-1479

44. Majetich, Sara A., Carter, Adriaan C., Belot, J., McCullough, Richard D., J. Phys. Chem. Vol. 98(51), 1994, 13705-13710

45. Veinot J., Ginzburg M., Pietro W.J., Chem. Nater. Vol. 9, 1997, 2117-2122

46. Sachleben J.R., Wooten E.W., Emsley L., Pines A., Chem. Phys. Lett. Vol. 198, 1992, 431-436

47. Dean P.A., Vittal J.J., Inorg. Chem., Vol. 25, 1986, 514-519

48. Fojtik, A., Weller, H., Koch, U., Henglein, A., Ber. Bunsen-Ges. Phys. Chem. Vol. 88(10), 1984, 969-977

49. Spanhel L., Weller H., Henglein A., J. Am. Chem. Soc. Vol. 109(22), 1987, 6632-6635.

50. Spanhel L., Weller H., Fojtik A., Henglein A., J. Ber. Bunsen-Ges. Phys. Chem. Vol. 91 (2), 1987, 88-94

51. Henglein A., Gutierrez M., Weller H., Fojtik A., Jirkovsky J., Ber. Bunsen-Ges. Phys. Chem. Vol. 93(5), 1989. 593-600

52. Hasselbarth A., Eychmuller A., Eichberger R., Giersig M., Mews A., Weller H., J. Phys. Chem. Vol. 97, 1993, 5333-5340

53. Dabbousi B.O., Rodriguez-Viejo J., Mikulec F.V., Heine J.R., Mattoussi H., Ober R.,

Jensen K.F., Bawendi M.G., J Phys. Chem. B Vol. 101, 1997, 9463-9475

54. Danek M., Jensen K.F., Murray C.B., Bawendi M.G., Chem. Mater. Vol. 8(1), 1996, 173-180

55. Peng X., Schlamp M.C., Kadavanich A.V., Alivisatos A.P., J. Am. Chem. Soc. Vol. 119, 1997, 7019-7029

56. Eychmueller A., Hasselbarth A., Weller H., J. Lumin. Vol. 53(1-6), 1992, 113-115

57. Kamalov V.F., Little R., Logunov S.L., El-Sayed M.A., J. Chem. Phys. Vol. 100(16), 1996, 6381-6384

58. Kumar A., Kumar S., Chem. Let., 1996, 711-712

59. Fox A.M., dulay M.T., J. Photochem. Photobiol., A Vol. 98(1-2), 1996, 91-101.

60. Chandler R.R., Coffer J.L., Atherton S.J., Snowden P.T., J. Phys. Chem. Vol. 96(6), 1992, 2713-2717

61. Chandler R.R., Coffer J.L., J. Phys. Chem. Vol. 95, 1991, 4-6

62. Hao E.C., zhang H., Yang B., Ren H., Shen J.C., Langmuir in press

63. Sun L.D., Liu C.H., Liao C.S., Yan C.H., J. Mater. Chem. Vol. 9, 1999, 1655-1657

64. Correa-Duarte M.A., Giersig M., Liz-Marzan L.M., Chemical Physics Letters, Vol. 286, 1998, 497-501

65. Suresh E., Bhadbhade M.M., Acta Cryst. C53, 1997, 193-195

66. Sullivan B.P., salmon D.J., Meyer T.J., Inorg. Chem., Vol. 17, 1978, 3334-3341

67. Little B.F., Long G.J., Inorg. Chem., Vol. 17, 1978, 3401-3405

68. Vossmeyer T., Katsikas L., Giersig M., Popovic I.G., Diesner K., Chemeseddine A., Eychmuller A., Weller H., J. Phys. Chem. Vol. 98, 1994, 7665-7673

69. Murray C.B., Norris D.J., Bawendi M.G., J. Am. Chem. Soc. Vol. 115, 1993, 8706-8715

70. Karlin K.D., Zukicta J.E., Biochemical and Inorganic Perspectives, Academic Press, NY, 1983

71. Peka P., Schula H.J., Physica B Vol. 193, 1994, 57-65

72. Yoffe A.D., Advances in Physics Vol. 42, 1993, 173-266

VITA

Tong Ni

Candidate for the Degree of
Master of Science

Thesis: SYNTHESIS, PROPERTY STUDY AND MODIFICATION OF II-VI SULFIDE SEMICONDUCTOR NANOPARTICLES

Major Field: Chemistry

Biographical:

Education: Graduated from Lanzhou University in 1992, received Bachelor of Science degree in Chemistry and Master of Science degree in Chemistry in June 1992, and in June 1995, respectively. Completed the requirements for the Master of Science degree with a major in Chemistry at Oklahoma State University in May, 2000.

Experience: Employed as an analytical chemist by Gansu State EPA Analytical Center, conducted environmental water, soil and gas sample preparation and analysis, QA/QC management. Employed by Oklahoma State University, Chemistry Department as a graduate teaching/research assistant.

Professional Memberships: American Chemical Society